

Unveiling the nature of the unidentified gamma-ray sources 4FGL J1908.6+0915e, HESS J1907+089/HOTS J1907+091, and 3HWC J1907+085 in the sky region of the magnetar SGR 1900+14

B. Hnatyk,^{1*} R. Hnatyk,¹ V. Zhdanov,¹ and V. Voitsekhovskiy¹

¹ *Astronomical Observatory, Taras Shevchenko National University of Kyiv, 3 Observatorna str. Kyiv, 04053, Ukraine*

Accepted XXX. Received YYY; in original form ZZZ

ABSTRACT

Supernova remnants (SNRs), star formation regions (SFRs), and pulsar wind nebulae (PWNe) are prime candidates for Galactic PeVatrons. The nonthermal high-energy (HE, $\varepsilon > 100$ MeV) and very high-energy (VHE, $\varepsilon > 100$ GeV) γ -ray emission from these sources should be a promising manifestation of acceleration processes. We investigate the possibility to explain the HE and VHE γ -ray emission from the sky region of the magnetar SGR 1900+14 as a signature of cosmic rays accelerated in above mentioned sources. To this end, we simulate the γ -ray emission from the extended *Fermi*-LAT HE source 4FGL J1908.6+0915e, the extended VHE H.E.S.S. source candidate HOTS J1907+091, and the point-like HAWC TeV source 3HWC J1907+085, which are spatially coincident with the SNR G42.8+0.6, the magnetar SGR 1900+14 and the star forming region W49A. The simulations are performed within the hadronic and leptonic models. We show that the observed γ -ray emission from the region of the magnetar SGR 1900+14 can, in principle, include contributions of different intensities from all three types of (potentially confused) sources. The considered in detail cases of a magnetar-connected but still undetected SNR and a PWN are the most promising ones, but with a serious requirement on the energy reserve of radiated CR particles - of order of $10^{51} d_{10\text{kpc}}^2$ erg for sources at a distance of $d \sim 10$ kpc. Such energy reserve can be provided by the magnetar-related Hypernova and/or magnetar wind nebula remnant created by the newborn millisecond magnetar with the large supply of rotational energy $E_{\text{rot}} \sim 10^{52}$ erg.

Key words: Stars: magnetars – ISM: supernova remnants – gamma rays: general – acceleration of particles – radiation mechanisms: non-thermal

1 INTRODUCTION

One of the major unsolved problems in modern astrophysics is the determination of sources and acceleration mechanism(s) of cosmic rays (CRs): Galactic ($E_{\text{cr}} \lesssim 10^{18}$ eV) and extragalactic ($E_{\text{cr}} \gtrsim 10^{17}$ eV) ones. (Berezinskii et al. 1990; Nagano & Watson 2000; Hillas 2005; Kotera & Olinto 2011; Blasi 2013; Neronov 2017) Ultra high energy CR (UHECR, $E_{\text{cr}} > 10^{18}$ eV) are believed to be of extragalactic origin, but some contribution from transient Galactic sources is also possible (Nagano & Watson 2000; Blasi et al. 2000; Arons 2003; Kotera & Olinto 2011; Berezhinsky 2014; Aloisio et al. 2014; Kotera et al. 2015; Alves Batista et al. 2019).

In potential Galactic sources of CRs – Supernova (SN) remnants (SNRs), Star formation regions (SFRs), and Pulsar wind nebulae (PWNe) – powerful shock waves can provide an effective diffusive shock acceleration (DSA) of protons, heavier nuclei with a charge $Z > 1$, and electrons/positrons

up to multi-PeV energies $E > 10^{15} Z$ eV (Hillas 2005; Ioka & Mészáros 2010; Bykov et al. 2020; Morlino et al. 2021).

Promising signatures of acceleration processes are expected to be a nonthermal high-energy (HE, $\varepsilon > 100$ MeV) and very high-energy (VHE, $\varepsilon > 100$ GeV) γ -ray emission and neutrino messenger from CR sources' neighbourhoods due to CR nuclei-target interstellar matter (ISM) nuclei inelastic collisions (thereafter *pp*-collisions) with a subsequent pion decay (hadronic scenario) and inverse Compton (IC) scattering of low energy background photons by ultrarelativistic electrons and positrons (leptonic scenario) (Stecker 1977; Aharonian 2004; Fox et al. 2013; Cristofari et al. 2018; Cherenkov Telescope Array Consortium et al. 2019; Fang & Murase 2021). Therefore, the observed spectra and morphology of γ -ray sources provide unique information about both the physical processes in the sources and the mechanisms of CR acceleration.

Recent observations of sky region of magnetar SGR 1900+14 reveal a set of new unidentified sources, especially in γ -ray band. They include the extended 4FGL J1908.6+0915e and three point-like J1908.7+0812,

* E-mail: bohdan_hnatyk@ukr.net

J1910.0+0904, J1911.0+0905 *Fermi*-LAT sources from the 4FGL Catalogue, based on the first eight years of observations from the *Fermi*-LAT Gamma-ray Space Telescope (Abdollahi et al. 2020), the extended source candidate (hotspot) HOTS J1907+091 detected in the High Energy Spectroscopic System (H.E.S.S.) Galactic plane survey (HGPS) (H. E. S. S. Collaboration et al. 2018a), and point-like source 3HWC J1907+085/2HWC J1907+084* from the 3HWC catalog of sources with energies above several TeV of the High Altitude Water Cherenkov (HAWC) observatory (Albert et al. 2020).

One of the potential candidates for these γ -ray sources is the magnetar SGR 1900+14 itself. Magnetars are young neutron stars with extremely high surface magnetic fields $B_s \sim 10^{14} - 10^{15}$ G (Duncan & Thompson 1992; Thompson & Duncan 1995, 1996; Turolla et al. 2015; Mereghetti et al. 2015; Kaspi & Beloborodov 2017; Esposito et al. 2021). Observed persistent X-ray – γ -ray activity of magnetars manifests in forms of repeated hard X-ray – soft γ -ray flares (soft gamma repeaters, SGRs) (Paczynski 1992; Thompson & Duncan 1995, 1996; Kouveliotou et al. 1998) and persistent/transient quiescent super-luminous X-ray emission, together with short (milliseconds-seconds) bursts and longer (weeks-months) outbursts (anomalous X-ray pulsars, AXPs) (van Paradijs et al. 1995; Thompson & Duncan 1996; Kaspi et al. 2003). The total magnetar luminosity considerably exceeds ordinary spin-down energy losses and is supported mainly by a decay of magnetar’s magnetic energy during a magnetic field evolution inside a neutron star or reconfigurations of magnetospheric fields (Thompson & Duncan 1995, 1996).

Large magnetic fields of magnetars result in a set of distinctive features of magnetars’ evolution in comparison with an ordinary pulsar case. Dissipation of a dipolar magnetic field energy ($E_{\text{mag}} \approx B_s^2 R_{\text{NS}}^3 / 6 \approx 3 \times 10^{47} B_{s,15}^2$ erg for the radius of neutron star $R_{\text{NS}} = 12$ km) supplies a X-ray – γ -ray activity of magnetars, including spectacular rare giant flares – the short (~ 0.1 s) hard X-ray – soft γ -ray bursts with luminosities $\sim 10^{44} - 10^{47}$ erg s $^{-1}$ and released energies $\sim 10^{44} - 10^{46}$ erg (from SGR 0526–66 on 1979 March 5, from SGR 1900+14 on 1998 August 27, and from SGR 1806–20 on 2004 December 27) (Olausen & Kaspi 2014). Hereafter the physical quantities are expressed by $Q = 10^n Q_n$ in cgs units, unless specified otherwise. A sudden release of magnetic energy in over-twisted magnetospheres via solar flare-like fast reconnections creates a GRB-like fireball and an ultrarelativistic (Lorentz factor $\gamma_j \lesssim 10$) outflow (Thompson & Duncan 1995; Parfrey et al. 2013), observed as radio afterglows of the SGR 1900+14 (Frail et al. 1999) and the SGR 1806–20 (Granot et al. 2006) giant flares.

Non-detection of reliable signatures of certainly present magnetar-connected SNR and magnetar wind nebula (MWN) can be explained by both the large distance of $d_{\text{mag}} \sim 12.5$ kpc and the large absorption in Galactic plane (Olausen & Kaspi 2014). Once more, owing to expected presence of relativistic shock waves and reconnection processes in newborn millisecond magnetar winds and magnetar giant flares, magnetars are promising accelerators of UHECRs (Blasi et al. 2000; Arons 2003; Eichler 2005; Asano et al. 2006; Liu et al. 2010; Kotera & Olinto 2011; Guépin & Kotera 2017; Fang et al. 2019). As argued in Gnatyk (2018), the magnetar SGR 1900+14 is a potential source of $E_{\text{cr}} > 10^{20}$ eV UHECR triplet (Sokolosky 2014) in view of joint data of Telescope Ar-

ray (TA) (Abbasi et al. 2014) and Auger (Aab et al. 2015) detectors. Reasonable association of the distant magnetar SGR 1900+14 with the 4 BCE "po star" (Wang et al. 2002) suggests a Hypernova type of a magnetar-related SN with favourable conditions for UHECR acceleration (Kotera & Olinto 2011). If this is the case, the magnetar SGR 1900+14 should also manifest himself as a PeVatron with nonthermal emission in different domains – from radio to TeV-range (Aharonian 2004; Cherenkov Telescope Array Consortium et al. 2019).

Besides SGR 1900+14, a list of possible source candidates includes two SNRs: SNR G42.8+0.6 and SNR G 43.3-0.2 from the Catalogue of Galactic Supernova Remnants (Green 2019) and star forming regions magnetar host stellar cluster Cl 1900+14 and W49A (Fig. 1). Possible source confusion should be also taken into account.

In our work we analyse all presently available multi-band observational data of the magnetar SGR 1900+14 region, including the high-energy and very high-energy γ -ray emission, detected by *Fermi*-LAT, H.E.S.S. and HAWC. We model the observational data in the frame of an expected hybrid multi-band emission from the all potential sources in this sky region: magnetar-connected SNR and MWN, SNRs G42.8+0.6 and W49B, SFRs Cl 1900+14 and W49A. Source confusion, especially due to TeV halos as a background sources, is considered as well. As follows from simulations, the most realistic models are connected with hadronic or leptonic γ -ray emission with the necessary supply of energy in hadronic or leptonic CR components of order of $10^{51} d_{10\text{kpc}}^{-2}$ erg. In the magnetar model the newborn magnetar SGR 1900+14 had to have a millisecond initial period in order to transmit $\sim 10^{52}$ erg into the SNR and/or MWN.

We are also reconstructing the evolutionary track of the magnetar progenitor star from its birth in a young compact cluster of massive stars Cl 1900+14 to its outburst as Hypernova and subsequent Hypernova remnant (HNR) evolution.

The paper is structured as follows. In Section 2 we describe multiwavelength observations of the sky region of the magnetar SGR 1900+14, from radio to γ -ray band. In Section 3 expected signatures of potential γ -ray sources in this region – SNRs, PWNe, and SFRs – are discussed. Modeling of multiband spectral energy distribution (SED) of observed HE and VHE γ -ray emission from the region of the magnetar SGR 1900+14 are presented as well. In Section 4 we present a comparative analysis of the expected contributions of potential sources to the total observed γ -ray emission. In Section 5 a comprehensive analysis of Hypernova model as the most appropriate one is presented. We focus on observational and theoretical arguments in support of the evolution scenario with the SGR 1900+14 progenitor as a Hypernova/Superluminous Supernova (SLSN). The discussion is presented in Section 6 and conclusions are summarised in Section 7.

2 MULTIWAVELENGTH OBSERVATIONS OF THE SKY REGION OF THE MAGNETAR SGR 1900+14

2.1 Sky region of SGR 1900+14 in the gamma-ray band

Search for persistent and pulsed γ -ray emission from 20 magnetars (including SGR 1900+14) in six years of *Fermi*-LAT

data was unsuccessful with upper limits $\sim 10^{-12} - 10^{-11}$ erg $\text{cm}^{-2} \text{s}^{-1}$ in the 0.1 – 10 GeV band (Li et al. 2017). At the same time, a positive result of this search was revealing of an extended γ -ray source positionally coincident with SGR 1900+14, as well as with the adjacent SNR G042.8+00.6. In the *Fermi*-LAT Fourth Source Catalogue (8-year Source Catalogue 4FGL, v19) (Abdollahi et al. 2020) this extended source 4FGL J1908.6+0915e with coordinates RA = $287^\circ.16$, Dec = $9^\circ.26$ ($l = 43^\circ.1249$, $b = 0^\circ.4301$), and radius of $\Theta_{\text{HE}} = 0^\circ.6$ has an overall significance only 4.58σ (5.8σ in 4FGL, v.27) (Fig. 1). Differential photon flux density of 4FGL J1908.6+0915e in the 50 MeV – 1 TeV energy range can be approximated by a power-law

$$F_{\text{ph}}(\varepsilon) = F_{\text{ph}}(\varepsilon_0)(\varepsilon/\varepsilon_0)^{-\Gamma}, \quad (1)$$

with the reference (pivot) energy $\varepsilon_0 = 4.52$ GeV, the normalization $F_{\text{ph}}(\varepsilon_0) = (1.01 \pm 0.19) \times 10^{-13}$ ph $\text{cm}^{-2} \text{s}^{-1} \text{MeV}^{-1}$ and the photon index $\Gamma = 2.23 \pm 0.098$. As a likely associated source the SNR G42.8+0.6 in this catalogue is noted.

Very recently Xin & Guo (2021) reported the connection of a pion-like source 4FGL J1910.2+0904c (Fig. 1) with the γ -ray emission around W49A – a massive star forming region in the Galaxy.

In the very high energy (VHE, $\varepsilon > 100$ GeV) γ -ray domain the H.E.S.S. Galactic Plane Survey (HGPS) (H. E. S. S. Collaboration et al. 2018a) reveals a source candidate (hotspot) HOTS J1907+091 with test statistics (TS) above TS = 30 detection threshold only in one (cross-check TS = 43) of two analyses (significance of TS = 18). Centred at $l = 42^\circ.88 \pm 0^\circ.08$, $b = 0^\circ.69 \pm 0^\circ.08$, HOTS J1907+091 has the measured integral photon flux $F_{\text{ph}}(\varepsilon > 1 \text{ TeV}) = 4.3 \times 10^{-13} \text{ cm}^{-2} \text{s}^{-1}$ and extension (radius) of $\Theta_{\text{VHE}} = 0^\circ.17 \pm 0^\circ.04$. For purpose of modelling we approximate the 1 – 10 TeV HOTS J1907+091 differential flux according to the *Fermi*-LAT power-law spectrum extension by a power-law spectrum with a photon index $\Gamma = 2.3 \pm 0.2$ and a standard deviation $\delta F = 0.2F$ (Figs. 3–7). Here we took into account that average index of known Galactic VHE γ -ray sources is $\Gamma = 2.3 \pm 0.2$ (H. E. S. S. Collaboration et al. 2018a).

Two potential counterparts of HOTS J1907+091 are spatially coincident with hotspot: the magnetar SGR 1900+14 and the SNR G42.8+0.6 (H. E. S. S. Collaboration et al. 2018a).

Using a blind search methods for γ -ray source detection based on image processing and pattern recognition techniques Remy et al. (2020) have recovered potentially valuable objects in the HGPS significance map. Set of objects around the SGR 1900+14 position recovering through an edge detection operator and a Hough circle transform correspond to the extended structure of the TeV source with partial circular symmetry (Fig. 1).

The closest source to SGR 1900+14 (a separation of $\approx 0^\circ.75$) in the 3HWC HAWC Observatory Gamma-Ray Catalogue (Albert et al. 2020) is a TeV point-like source 3HWC J1907+085 with coordinates RA = $286^\circ.79$, Dec = $8^\circ.57$ ($l = 42^\circ.35$, $b = 0^\circ.44$), (all with $1\sigma_{\text{stat}} = 0^\circ.09$), a somewhat low TS = 75.5 peak on an extended background spot (with 2HWC J1907+084* counterpart in the 2HWC Catalogue Abeysekara et al. 2017).

In the 3HWC peak sensitivity region (~ 10 TeV) the best-fit parameters of the 3HWC J1907+085 power-law γ -ray spectrum are: the reference (pivot) energy $\varepsilon_0 = 7$ TeV,

the normalization $F(\varepsilon_0) = (8.4^{+0.9}_{-1.0} {}^{+2.5}_{-1.62}) \times 10^{-15} \text{ TeV}^{-1} \text{ cm}^{-2} \text{s}^{-1}$ and the photon index $\Gamma = 2.95 \pm 0.09 {}^{+0.04}_{-0.09}$. A shell-like (necklace) structure (with 3HWC J1907+085/2HWC J1907+084* as the brighter knot ($\sigma \sim 5$)), overlapping SGR 1900+14, the SNR G42.8+0.6 and H.E.S.S. HOTS J1907+091, are clearly visible in the γ -ray $\sigma \geq 3$ excess map with subtracted γ -ray contribution from the spatially extended source MGRO J1908+06 (see Extended Data Fig. 1 in Abeysekara et al. 2018).

There are no other potential counterparts of 3HWC J1907+085. The nearest ($\sim 0^\circ.3$) pulsar in the Australia Telescope National Facility Pulsar Catalogue (ATNF) of 1509 pulsars Manchester et al. (2005) PSR J1908+0839 (period $P = 0.185$ s, distance $d = 8.27$ kpc, characteristic age $\tau_c = 1.23$ Myr, spin down power $\dot{E} = 1.5 \times 10^{34} \text{ erg s}^{-1}$) is too old and too slow rotating in order to support the necessary TeV luminosity of putative PWN (Ahnen et al. 2019).

In recent work (Abdalla et al. 2021) the H.E.S.S. Collaboration presented a new analysis for the H.E.S.S. data and declared that the the hotspot HOTS J1907+091 is a real new H.E.S.S. source HESS J1907+089, namely, it is the H.E.S.S. detection of HAWC J1907+085 source.

To summarise, as the observationally confirmed in the region of the magnetar SGR1900+14 we can consider only extended HE and VHE γ -ray sources: the *Fermi*-LAT source 4FGL J1908.6+0915e, the H.E.S.S. source HESS J1907+089/HOTS J1907+091, and similar hotspot around HAWC point-like source 3HWC J1907+085/2HWC J1907+084* (Fig. 1).

2.2 SGR 1900+14 region in the radio band

The radio map of SGR 1900+14 region does not display any signatures of the magnetar, as well as of a magnetar-connected SNR or a MWN, only 3σ limits on an extended emission of $6.1 \text{ mJy arcmin}^{-2}$ (332 MHz) and $6.2 \text{ mJy arcmin}^{-2}$ (1.4 GHz) were found in Kaplan et al. (2002) (Figs. 3–7). In the proximity to SGR 1900+14 there is only in radio-band detected shell-type SNR G42.8+0.6 (of $24'$ size, $l = 42^\circ.820$, $b = 0^\circ.635$, spectral flux density $F_\nu = 2.4 \pm 0.6 \text{ Jy}$ at 1.420 GHz, $2.0 \pm 0.2 \text{ Jy}$ at 2.695 GHz, $1.5 \pm 0.2 \text{ Jy}$ at 4.750 GHz, spectral index $\alpha = 0.4$) (Fuerst et al. 1987). The angular separation between the magnetar and the centre (boundary) of the SNR G42.8+0.6 is of $\sim 15' (3')$ (Fig. 1). Young ($\tau_c \approx 38 \text{ kyr}$) $P = 226 \text{ ms}$ radio pulsar PSR J1907+0918 ($l = 43^\circ.024$, $b = 0^\circ.730$ $d = 8.2 \text{ kpc}$), is a neighbour of SGR 1900+14, the separation between the pulsars $\approx 2'$ (Lorimer & Xilouris 2000; Kaplan et al. 2002). Despite the young age of both pulsars, none of them is physically connected with the SNR G42.8+0.6 in view of unrealistically high necessary transverse velocity $v_t = 4 \times 10^3 (d_p/10 \text{ kpc}) / (t_p/10^4 \text{ yr}) \text{ km s}^{-1}$ for expected distances $d_p \sim 5 - 15 \text{ kpc}$ and ages $t_p \sim 10^3 - 4 \times 10^4 \text{ yr}$ of pulsars (Kouveliotou et al. 1999; Lorimer & Xilouris 2000). Moreover, the estimated proper motion of SGR 1900+14 (Tendulkar et al. 2012) corresponds to $v_t = (104 \pm 24) \times (d_p/10 \text{ kpc}) \text{ km s}^{-1}$ and to the approach to the SNR with position angle PA = $254^\circ \pm 10^\circ$. Recent estimate of the extinction-based distance to the SNR G42.8+0.6 $d_{\text{ext}} = 4.24 \pm 0.93 \text{ pc}$ (Wang et al. 2020) also excludes its physical connection with SGR 1900+14.

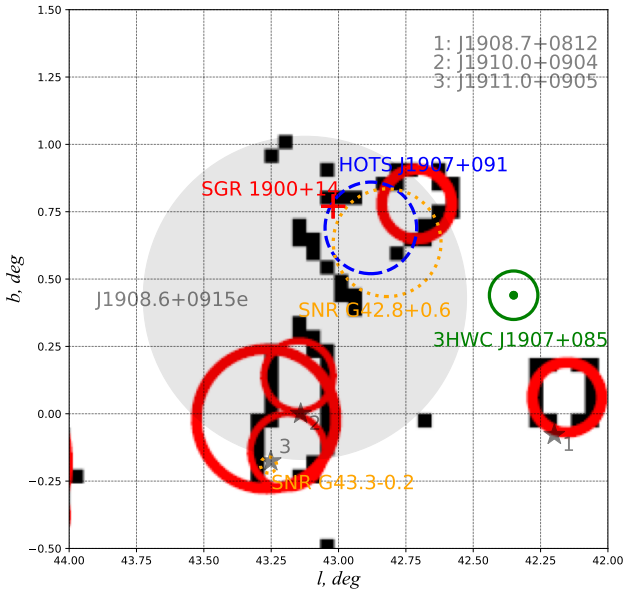


Figure 1. Sky region of the magnetar SGR 1900+14. The red cross indicates the SGR 1900+14 position. The extended 4FGL source J1908.6+0915e (the grey circle) and three point-like 4FGL sources (the grey stars) are also presented together with the H.E.S.S. extended source HOTS J1907+091 (the blue ring) and the HAWC point-like source 3HWC J1907+085 (the green bullet with 1σ error box). Two SNRs in the field are presented by the orange rings. The star forming region W49A coincides with the star 2. The black filled squares correspond to the edge mask and the red circles to the objects detected in Hough space in H.E.S.S. data, respectively. See text for details.

The second, more distant ($\sim 1^\circ$) from the magnetar, shell-type SNR G43.3-0.2 (W49B), of $4' \times 3'$ size at distance $d = 11.3$ kpc, $l = 43^\circ.275$, $b = -0^\circ.190$, spectral flux density $F_\nu = 38$ Jy at 1 GHz, spectral index $\alpha = 0.46$ (Green 2019) is detected also in X-ray and γ -ray range as a young (age $t \approx 6$ kyr) compact (radius $R \approx 8$ pc) SNR – effective cosmic ray accelerator with the proton CR energy $W_{\text{cr},p} \approx 2 \times 10^{49}$ erg), evolving in a dense (the number density $n_{\text{mc}} \approx 650$ cm^{-3}) molecular cloud (see Sano et al. (2021) and references therein). Due to large separation (more than 1 kpc) W49B does not belong to the SGR 1900+14 neighborhood.

2.3 SGR 1900+14 region in the optical/infrared band

Initial searches for a SGR 1900+14 counterpart in the optical/infrared (IR) region were unsuccessful: HST/STIS, and Keck J/Ks-band images placed only upper limits of $m_{50\text{CCD}} \gtrsim 29.0$ mag, $J \gtrsim 22.8$ mag, $K_s \gtrsim 20.8$ mag (Kaplan et al. 2002). Only in Testa et al. (2008) a newly detected variable "object # 7" with $K_s \approx 19.7$ mag and $\Delta K_s = 0.47 \pm 0.11$ mag, observed with ESO-VLT/NACO in the error circle of the SGR 1900+14 radio position, was proposed as a tentative IR candidate counterpart to SGR 1900+14. Later on, "Star 7" was confirmed by Keck 2 LGS-AO/NIRC2 observation as the IR counterpart (Tendulkar et al. 2012).

Tendulkar et al. (2012) confirmed claimed in Vrba et al. (1996, 2000) physical connection of the magnetar with the young compact of radius $R_{\text{cl}} \approx 0.4 - 0.6$ pc embedded cluster of massive stars Cl 1900+14, aka SGR 1900+14 Star Cluster (Morales et al. 2013), with two luminosity-dominated M5 Red Supergiant (RSG) and a few Blue Supergiant (BSG) stars and improved in Davies et al. (2009) distance $d_{\text{cl}} = 12.5 \pm 1.7$ kpc and extinction $A_V = 12.9 \pm 0.5$ mag. In view of the distance, having the transverse velocity $v_t = 130 \pm 30$ km s^{-1} , it is possible to estimate the age of the magnetar which needs 6 ± 1.8 (3 ± 0.9) kyr to escape from its birthplace at the centre (edge) of the cluster.

An additional confirmation of a physical connection of the magnetar with the cluster is based on the IR elliptical shell around SGR 1900+14 (Fig. 2), discovered by Wachter et al. (2008) in Spitzer $16 \mu\text{m}$ and $24 \mu\text{m}$ images. Wachter et al. (2008) suggested that this shell is a signature of a dust-free cavity produced by the giant flare of SGR 1900+14 in the stellar cluster-connected dusty gas on 1998 August 27. Observed shell dust temperature of $80 - 120$ K and IR flux of 1.2 ± 0.2 Jy and 0.4 ± 0.1 Jy at $24 \mu\text{m}$ and $16 \mu\text{m}$, respectively, together with the absence of ring signatures at optical, near-IR, radio- or X-ray wavelengths, was explained in a model of a dust heating by the embedded star cluster without the possible presence of a shock wave from the SN explosion. The 3D dust radiative transfer modelling (Natale et al. 2017) reproduces observational data in a model of a cavity in a circumcluster medium with a sharp inner boundary and a molecular cloud-like extinction, with two illuminating RSG stars inside the cavity. The necessary total mass of the radiating dust is $M_{\text{dust}} \sim 2M_\odot$ and the cloud gas number density $n_{\text{mc}} \sim 10^3$ cm^{-3} for a dust-to gas ratio of 0.00619. Resulting high gas number density at the cavity boundary leads to the total mass of gas inside the IR shell of radius ~ 1.5 pc and of volume ~ 13 pc^3 of order of $400M_\odot$ and the total mass of gas outside the cavity $\sim 320M_\odot$, or the total mass of a putative molecular cloud of radius ~ 2 pc $M_{\text{mc}} \gtrsim 10^3M_\odot$, but such a molecular cloud is still not observed. In the Catalogue of 695 embedded and open stellar clusters in the inner Galaxy VizieR J/A+A/560/A76 (Morales et al. 2013) the cluster Cl1900+14/SGR 1900+14 is classified as an "OC2: open cluster without gas and without ATLASGAL survey counterpart". In a complete sample of ~ 8000 $M_{\text{mc}} \gtrsim 10^3M_\odot$ dense clumps located in the Galactic disc ($5^\circ < l < 60^\circ$) ATLASGAL (Urquhart et al. 2018) an angular separation with the closest clump is of $0^\circ.8$ (G043.141-00.01), whereas in the all-Galaxy CO survey ($M_{\text{mc}} \gtrsim 3 \times 10^3M_\odot$ in the outer Galaxy) (Rice et al. 2016) the closest molecular cloud with $l = 43^\circ.553$, $b = 0^\circ.567$ is of $0^\circ.57$ away.

Therefore in Section 5.3 we propose and substantiate a new model of observed IR emission from the relics (debris) of dusty magnetar-related SN ejecta (Fig. 2).

2.4 SGR 1900+14 region in the X-ray band

In the X-ray domain, after the giant flare in 1998 and two re-brightening in 2001 and 2006, SGR 1900+14 returned to minimum quiescent flux level with the typical for magnetars two-component spectrum: a black body component with temperature of $k_B T = 0.52$ keV and a hard power-law component with photon index $\Gamma = 1.21$. For a column density of $N_{\text{H}} = 1.9 \times 10^{22}$ cm^{-2} , the quiescent bolometric luminosity

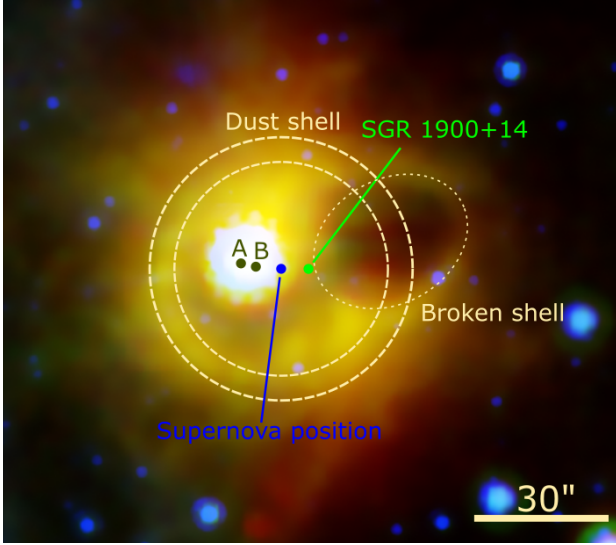


Figure 2. Spitzer IR map of SGR 1900+14 environment with colour coding: blue ($8\ \mu\text{m}$), green ($16\ \mu\text{m}$), and red ($24\ \mu\text{m}$) (courtesy NASA/JPL/Caltech/S. Wachter (Caltech-SSC)). We indicated with the green bullet the present magnetar position and with the black bullets A and B – the positions of two RSGs at the centre of the open star cluster Cl 1900+14/SGR 1900+14. In our model, the blue bullet in the centre of the observed dust shell (the yellow dashed ring) indicates the Supernova position 2 kyr ago, whereas the broken shell (the yellow dotted ellipse) has been created by the anisotropic giant flare on 1998 August 27. See text for details.

is of $L_{\text{bol}} = 5.6 \times 10^{35}\ \text{erg s}^{-1}$ (Turolla et al. 2015; Enoto et al. 2017; Coti Zelati et al. 2018; Tamba et al. 2019). Recent analysis of XMM-Newton and NuSTAR data (Tamba et al. 2019) has revealed a monotonic decrease in the 1 – 10 keV flux and the spin-down rate \dot{P} in 2006-2016. Newly obtained values $P = 5.22669(3)\ \text{s}$, $\dot{P} = 3.3 \times 10^{-11}\ \text{s s}^{-1}$ for 2016 correspond to magnetar magnetic field $B_s = 4.3 \times 10^{14}\ \text{G}$ and the characteristic age $\tau_c \approx 2.4\ \text{kyr}$ (cf. the old value $\tau_c \approx 700\ \text{yr}$). No signatures of an adjacent SNR or MWN were detected yet in the X-ray band.

We adopted the intrinsic (unabsorbed) 2 – 10 keV flux of SGR 1900+14 $F_{2-10\ \text{keV}} = 1.8 \times 10^{-12}\ \text{erg cm}^{-2}\text{s}^{-1} = 1.1 \times 10^{-9}\ \text{GeV cm}^{-2}\text{s}^{-1}$ (Tamba et al. 2019) as an upper limit for expected SNR/MWN 2-10 keV flux.

3 EXPECTED SIGNATURES OF SNRS, SFRS AND PWNE IN THE SGR 1900+14 REGION

Detected in the SGR 1900+14 region HE and VHE γ -ray sources: extended ones 4FGL J1908.6+0915e and HOTS J1907+091, as well as point-like peaks on enhanced background 3HWCJ1907+085/2HWCJ1907+084* and HESS J1907+089 correspond to three potential acceleration places of relativistic hadrons and leptons: SNRs, SFRs and PWNe. Due to presence of powerful shock waves with effective diffusive shock acceleration of CRs they are prominent Galactic PeVatrons – accelerators of protons, heavier nuclei and electrons/positrons up to PeV-energies. In observations, they are manifested by nonthermal radiation, especially, by HE and VHE γ -ray emission.

3.1 SNRs, SFRs and PWNe as CR accelerators

3.1.1 SNRs as CR accelerators

There are at least two SNRs in the SGR 1900+14 region: SNR G042.8+0.6 and the SNR of a SN that gave birth to a magnetar but has not yet been identified (Fig. 1). Indeed, magnetar SGR 1900+14, like other neutron stars, is a compact remnant of core collapse SN explosion.

In a case of an ordinary SN explosion a SN ejecta with a typical kinetic energy $W_{\text{ej}} \sim 1\ \text{Bethe (B)} = 10^{51}\ \text{erg}$ (from 0.09 to 2.3 B for 9-27 M_{\odot} progenitors) interacts with circumstellar/interstellar medium (ISM), creating shock-bounded expanding bubble of swept-up ISM gas – SNR – with energy reserve of $W_{\text{SNR}} \sim W_{\text{ej}} \sim 10^{51}\ \text{erg}$. A newborn neutron star – typical radio pulsar with a magnetic field $B_s \sim 10^{12}\ \text{G}$, a rotational period $P_i \sim 0.01 - 0.1\ \text{s}$ and a rotational energy $E_{\text{rot}} \sim 10^{48} - 10^{50}\ \text{erg}$, creates a termination shock (TS)-bounded PWN inside the SNR with an energy reserve of $W_{\text{PWN}} \lesssim E_{\text{rot}} \lesssim 10^{50}\ \text{erg}$ (see Burrows & Vartanyan (2021) and references therein).

SNRs are effective accelerators of Galactic CRs (of both hadronic (protons and nuclei) and leptonic (electrons) components) via DSA of charged ISM particles at SNR shocks.

The expected spectra of shock-accelerated nuclei (mainly, protons, $i = p$) and electrons ($i = e$) are of power-law (PL) or exponential cut-off power-law (ECPL) type

$$N_i(E_i) = N_{0,i}(E_i/E_{0,i})^{-\Gamma_{\text{cr},i}} \exp(-E_i/E_{\text{cut},i}), \quad (2)$$

where $E_{0,i}$ is the CR reference energy, $N_{0,i}$ is the normalisation, $N_{0,e}(E) = K_{ep}N_{0,p}(E)$, K_{ep} is the electron-to-proton energy fraction, $\Gamma_{\text{cr},i}$ and $E_{\text{cut},i}$ are the spectral index and the cut-off energy of i -th component, respectively. Classical value for spectral index in Fermi-I nonrelativistic shock acceleration is $\Gamma_{\text{cr},i} = 2$, in case of relativistic parallel shocks $\Gamma_{\text{cr},i} = 2.2$ (Kirk & Duffy 1999; Kirk et al. 2000). Observations of Galactic CR sources, e.g. radio-sources with spectral energy flux $F_{\varepsilon} \propto \varepsilon^{-\alpha}$ with $\alpha = \Gamma + 1 = (\Gamma_{\text{cr},e} - 1)/2 \approx (0.6 - 0.8)$ and diffuse Galactic CR background correspond to $\Gamma_{\text{cr},i} = 2.2 - 2.5$ (Stecker 1971; Berezhinskii et al. 1990; Hillas 2005; Delahaye et al. 2010; Ferrand & Safi-Harb 2012; Yuan et al. 2017; Pelletier et al. 2017; Evoli et al. 2021).

The total energy of CR $W_{\text{cr},i}$ ($i = p, e$) is

$$W_{\text{cr},i} = \int_{E_{\text{min},i}}^{E_{\text{max},i}} EN_{0,i}(E/E_{0,i})^{-\Gamma_{\text{cr},i}} \exp(-E/E_{\text{cut},i}) dE, \quad (3)$$

and accelerated at SNR shock CR components include hadrons with total energy $W_{\text{cr},p} = \eta_{\text{cr}} W_{\text{SNR}}$ and leptons with total energy $W_{\text{cr},e} = K_{ep} W_{\text{cr},p}$, where $\eta_{\text{cr}} \sim 0.1$ is the efficiency of CR acceleration.

In typical SNR with $W_{\text{SNR}} \sim 10^{51}\ \text{erg}$ we expect $W_{\text{cr},p} \sim 0.1\eta_{p,-1}W_{\text{SNR}} \sim 10^{50}\eta_{p,-1}\ \text{erg}$, $W_{\text{cr},e} \sim 0.01K_{ep,-2}W_{\text{cr},p} \sim 10^{48}K_{ep,-2}\ \text{erg}$ for young SNR (age $t_{\text{SNR}} \lesssim 10^4\ \text{yr}$) with radius of $R_{\text{SNR}}(t \sim 10^3\ \text{yr}) \lesssim 10\ \text{pc}$ (Truelove & McKee 1999; Reynolds 2008). Hereafter the physical quantities are expressed by $Q = 10^n Q_n$ in cgs units, unless specified otherwise.

Maximum energy of the SNR diffusive shock-accelerated CRs with charge Ze , velocity $V_{\text{sh}} = \beta_{\text{sh}} \cdot c$ and shock-compressed ISM magnetic field $B_{\text{sh}} = \sqrt{11}B_{\text{ISM}}$ is (Hillas 2005):

$$E_{\text{max}} \approx Ze\beta_{\text{sh}}R_{\text{SNR}}B_{\text{sh}} \approx 3 \times 10^2 Z\beta_{\text{sh},-2}R_{\text{SNR},19}B_{\text{sh},-5}\ \text{TeV},$$

(4)

or $E_{\max} \approx 0.9Z$ PeV in our case.

Accelerated CRs, accumulated in a downstream region, are subject to adiabatic losses due to nonzero divergence of SNR plasma expansion velocity \bar{v} (Martín et al. 2012):

$$\dot{E}_{i,\text{ad}} = -\frac{1}{3}(\nabla \cdot \bar{v})E_i. \quad (5)$$

In a spherically symmetric SNR $E_i \propto R_{\text{SNR}}^{-1} \propto t_{\text{SNR}}^{-0.4}$, and the adiabatic loss time $t_{\text{ad}} = (E_i/\dot{E}_i)_{\text{ad}} = 2.5t_{\text{SNR}}$ exceeds the SNR age. At the same time, hadronic CRs diffusively escaping into upstream region with density enhancement $n_{\text{ISM}} \gtrsim 1 \text{ cm}^{-3}$ are noticeably losing energy in collisions with ISM protons and nuclei. For proton-proton collision cross-section $\sigma_{pp} = 40 \text{ mb}$ and the coefficient of inelasticity - part of proton energy lost in interaction - $\kappa \approx 0.5$ the cooling time is $t_{pp} = (\kappa n_{\text{ISM}} \sigma_{pp} c)^{-1} \approx 1.7 \times 10^{15} n_{\text{ISM}} \text{ s}$ (Aharonian 2004). Produced in collisions secondary pions rapidly decay into leptons, in particular, hadronic mechanism of γ -ray generation is connected with neutral pion decay $pp \rightarrow \pi^0 \rightarrow \gamma\gamma$. In the hadronic $E_p \gtrsim 10 \text{ GeV}$ scenario CR protons with energy $E_p \gtrsim 10 \text{ GeV}$ produce γ -ray photons with energy $\varepsilon \approx 0.1E_p$ and CR protons with power-law spectrum (2) produce power-law spectrum of γ -ray photons (1) with the spectral photon index $\Gamma = \Gamma_{\text{cr},p}$. Time scale for γ -ray production is $t_{pp,\gamma} = (\kappa_{\pi^0} n_{\text{ISM}} \sigma_{pp} c)^{-1} \approx 5 \times 10^{15} n_{\text{ISM}} \text{ s}$, where $\kappa_{\pi^0} \approx 0.17$ is the fraction of proton kinetic energy transferred to π^0 (Stecker 1971; Berezhinskii et al. 1990; H. E. S. S. Collaboration et al. 2018c).

Ultra high energy protons with Lorentz factor γ_p such that energy of background photon ε in proton rest frame $\varepsilon' = \gamma_p \varepsilon > 145 \text{ MeV}$ produce mesons (pions) in proton-photon collisions $p + \gamma \rightarrow p + \pi^0$, $p + \gamma \rightarrow n + \pi^+$. For CMB photons with $\varepsilon_{\text{CMB}} \approx 3k_B T_{\text{CMB}} \approx 7 \times 10^{-4} \text{ eV}$, where k_B is the Boltzmann constant, $\gamma_p \geq 10^{11}$. Cooling time for photopion production is $t_{p\gamma} = (\kappa_{p\gamma} n_{\gamma} \sigma_{p\gamma} c)^{-1} \approx 1.2 \times 10^{15} (n_{\gamma}/n_{\text{CMB}})^{-1} \text{ s}$, where $\kappa_{p\gamma} \approx 0.2$ is the coefficient of inelasticity and $\sigma_{p\gamma} \approx 340 \mu\text{b}$ is the cross-section for the photopion production (Stecker 1971; Berezhinskii et al. 1990). For Galactic CRs accelerated at SNR shocks a photopion production is negligible.

Energy losses of protons due to nonthermal (synchrotron and IC) radiation are $(m_p/m_e)^4 \approx 1.1 \times 10^{13}$ times smaller than the losses of electrons of the same energy (see detail below).

Observable spectra of hadronic γ -ray emission are determined by parameters of hadronic CR spectra (2) and number densities of target ISM particles n_{ISM} (Acero et al. 2016; Cristofari et al. 2018; H. E. S. S. Collaboration et al. 2018a).

3.1.2 SFRs as CR accelerators

Galactic SFRs, that include stellar clusters, OB associations, and superbubbles, are also promising sources of Galactic CRs and potential Galactic PeVatrons (Bykov et al. 2020; Morlino et al. 2021; Cristofari 2021, and references therein).

In the SGR 1900+14 region there are two SFRs: magnetar-connected star cluster Cl 1900+14 and a W49 complex that consists of a star forming region W49A and a SNR W49B (the last one outside the region considered) (Fig. 1).

In SFRs a common action of powerful winds of massive stars and SN ejectas leads to formation of a set of strong individual and large-scale termination shocks. Analogously to

the considered above SNR case, DSA is effective here and provides power-law type of CR spectra with spectral indexes $\Gamma_{\text{cr}} = 2 - 2.3$. Once more, a presence of multiple shocks increases the efficiency of CR acceleration and their maximum energies (Bykov et al. 2020). VHE γ -ray emission have been detected from some SFRs including magnetar SGR 1806-20-connected star cluster Cl*1806-20 (H. E. S. S. Collaboration et al. 2018b,e; Morlino et al. 2021).

3.1.3 PWNe as CR accelerators

PWNe are also effective accelerators of CRs, but mainly of their leptonic (electron and positron) components as dominant pulsar wind constituents via DSA at the relativistic TS (Gaensler & Slane 2006; Bucciantini et al. 2011; Amato 2014; Kargaltsev et al. 2015; Blondin & Chevalier 2017; Reynolds et al. 2017; H. E. S. S. Collaboration et al. 2018b; Zhu et al. 2018; Amato 2020), as well as via a driven magnetic reconnection (MR) and a resonant absorption of ion-cyclotron waves (Amato 2014, 2020).

Complex nature of lepton CR acceleration in PWN case does not allow to reliably determine CR spectral characteristics. The present relativistic leptonic component of CRs in PWNe is the result of the time-dependent TS/MR acceleration and cooling/escaping/advection processes (H. E. S. S. Collaboration et al. 2018b; Zhu et al. 2018, and references therein). The observed SED in PWNe is the sum of leptonic contributions from different injection epochs and space localisation. In this case a typical leptonic exponential cut-off broken power-law (ECBPL) spectrum

$$N_e(E_e) = \begin{cases} N_{0,e}(E_e/E_{0,e})^{-\Gamma_{1,\text{cr},e}}, & E_e < E_{\text{br},e} \\ N_{0,e}(E_{\text{br},e}/E_{0,e})^{(\Gamma_{2,\text{cr},e}-\Gamma_{1,\text{cr},e})}(E_e/E_{0,e})^{-\Gamma_{2,\text{cr},e}} \\ \quad \times \exp(-E_e/E_{\text{cut},e}), & E_e \geq E_{\text{br},e} \end{cases} \quad (6)$$

with characteristic break energy $E_{\text{br},e}$ and two PL spectra with $\Gamma_{1,\text{cr},e} < 2$ for $E_e \leq E_{\text{br},e}$ and $\Gamma_{2,\text{cr},e} > 2$ for $E_e \geq E_{\text{br},e}$ is widely used in PWN modelling (e.g. Torres et al. 2014; Ishizaki et al. 2017).

Acceleration of leptonic components in young ($t \lesssim t_{\text{sd},i}$) PWNe is very efficient. Considerable part η_e of spin-down luminosity L_{sd} is converted into CR lepton energy $W_{\text{cr},e}$: $\eta_e = W_{\text{cr},e}/L_{\text{sd}} \lesssim 1$, but energy losses of accelerated leptons result in an actual (derived from observations) value of $W_{\text{cr},e} \lesssim 10^{49} \text{ erg}$ (H. E. S. S. Collaboration et al. 2018b, and references therein).

Maximum energy of CR leptons, accelerated at relativistic TS with the TS velocity $\beta_{\text{TS}} = V_{\text{TS}}/c \approx 1$, the radius of PWN $R_{\text{PWN}} \sim 10^{19} \text{ cm}$, and the magnetic field inside it $B_{\text{PWN}} \sim 100 \mu\text{G}$ is considerably smaller than $\sim 300 \text{ PeV}$, predicted by (2) due to their severe energy losses inside PWN.

Relativistic electrons in the SNR/SFR case and electrons/positrons the PWN case (hereafter we use the term electrons to the both electrons and positrons in the last case) interact with magnetic fields of energy density $w_B = B^2/8\pi$ and with components of background radiation with energy density $w_{\text{rad},i}$: cosmic microwave background ($i = \text{CMB}$), infrared ($i = \text{IR}$), star light ($i = \text{SL}$) radiation, producing synchrotron (in the radio – X-ray band) and IC – synchrotron self-Compton (SSC) (in the GeV – TeV band) emis-

sion. (Gaensler & Slane 2006; Kargaltsev et al. 2015; Zhu et al. 2018; Amato 2020).

For a relativistic electron with the Lorentz factor $\gamma_e \gg 1$ and energy $E_e = \gamma_e m_e c^2$ the rate of energy losses is

$$P(E_e) = -\frac{dE_e}{dt} = \frac{4}{3} \sigma_T c (w_B + \sum_i w_{\text{rad},i} f_{\text{KN},i}(E_e, T_i)) \gamma_e^2, \quad (7)$$

where σ_T is the Thomson cross-section and

$$f_{\text{KN},i} = \frac{45K^2/64\pi^2}{45K^2/64\pi^2 + \gamma_e^2}, \quad (8)$$

where $K = m_e c^2 / k_B T_i$ and T_i is the temperature of the i -th component of background radiation ($i = \text{CMB, IR, SL}$), describes transition to Klein-Nishina scattering (Evoli et al. 2020, and references therein). From (7) it follows that electron energy loss time in the Thomson regime for synchrotron emission is

$$t_{\text{syn}}(\gamma_e) = \frac{E_e}{P_{\text{syn}}(E_e)} = \frac{6\pi m_e c}{\sigma_T B^2 \gamma_e} = 2.4 \times 10^1 B_{-5}^{-2} \gamma_{e,7}^{-1} \text{ kyr}, \quad (9)$$

whereas the energy loss time for IC emission is

$$t_{\text{IC},i}(\gamma_e) = \frac{3m_e c}{4\sigma_T w_{\text{rad},i} \gamma_e} = 2.6 \times 10^2 \frac{w_{\text{rad,CMB}}}{w_{\text{rad},i}} \gamma_{e,7}^{-1} \text{ kyr}. \quad (10)$$

Here $w_{\text{rad,CMB}} = 0.26 \text{ eV cm}^{-3}$ and $B_{\text{CMB}} = (8\pi w_{\text{rad,CMB}})^{1/2} = 3.2 \mu\text{G}$.

Advecting in downstream flow CR electrons suffer also from adiabatic losses with adiabatic time loss (5) determined by PWN radius R_{PWN} and flow velocity V_{PWN} : $t_{\text{ad,PWN}} = R_{\text{PWN}}/V_{\text{PWN}}$ (Martín et al. 2012).

Maximum energy of CR electrons in PWNe is determined by the balance of acceleration and loss processes. Characteristic acceleration time of CR with energy E and Larmor radius $r_L = E/ZeB$ in magnetic field B in diffusive shock acceleration at SNR shock wave of velocity $V_{\text{sw}} = \beta_{\text{sw}} c$ in Bohm diffusion regime with diffusion coefficient $D_B = r_L c/3$ is $t_{\text{acc}} = 8D_B/V_{\text{sw}}^2 = 8r_L/3\beta_{\text{sw}}^2 c$ (Evoli et al. 2021). Similar value $t_{\text{acc}} \approx r_L/c$ is expected in PWNe with relativistic TS (Pelletier et al. 2017). For most important synchrotron losses maximum energy of CR electron $E_{e,\text{max}} = \gamma_{e,\text{max}} m_e c^2$ follows from equality $t_{\text{acc}} = t_{\text{syn}}$:

$$\gamma_{e,\text{max}} = \frac{3m_e c^2}{2e^{3/2} B^{1/2}} = 3.8 \times 10^{10} B_{-5}^{-1/2}. \quad (11)$$

Observable spectra of leptonic γ -ray emission are determined by parameters of leptonic CR spectra (6) and background radiation (H. E. S. S. Collaboration et al. 2018b).

We note also that in young SNRs, including a magnetar-connected one, hadronic and leptonic emission are generated in a slow cooling regime. Both the hadronic energy loss time for inelastic pp collisions $t_{pp,\gamma} \approx 1.7 \times 10^5 (n_{\text{ISM}}/1 \text{ cm}^{-3})^{-1} \text{ kyr}$ and the leptonic cooling time for synchrotron and IC channels $t_i \approx 1.3 \times 10^2 (w_{\text{rad,CMB}}/w_{\text{rad},i})(E_e/10 \text{ TeV})^{-1} \text{ kyr}$ ($i = \text{CMB, IR, SL}$) exceed the magnetar age $t_{\text{mag}} \approx 2 \text{ kyr}$ for $E_e \lesssim 100 \text{ TeV}$.

3.2 Energy requirements for gamma-ray sources in the SGR 1900+14 region

To begin with, we assess the energy requirements for potential sources of observed GeV-TeV emission from SGR 1900+14 outskirts.

To this end, we use the recipe proposed in H. E. S. S. Collaboration et al. (2018c). In the leptonic scenario only IC emission from CMB photon scattering in Thomson regime is considered.

In the hadronic emission scenario, the γ -ray emission from HOTS J1907+091 can be explained as a result of pp interactions of SNR/SFR shock-accelerated protons and heavy nuclei with the target nuclei of ISM plasma.

For the mentioned above HOTS J1907+091 integral photon flux $F_{\text{ph}}(\varepsilon > 1 \text{ TeV}) = 4.3 \times 10^{-13} \text{ cm}^{-2} \text{ s}^{-1}$ the corresponding integral energy flux is $F_\varepsilon(\varepsilon > 1 \text{ TeV}) = 2.3 \text{ TeV} \times F_{\text{ph}}(\varepsilon > 1 \text{ TeV}) = 9.9 \times 10^{-13} \text{ TeV cm}^{-2} \text{ s}^{-1}$ for the spectral index $\Gamma = 2.3$. The necessary energy of accelerated CR protons with $E_p > 10 \text{ TeV}$ is:

$$W_{\text{cr},p}(E_p > 10 \text{ TeV}) \sim 4\pi d^2 F_\varepsilon(\varepsilon > 1 \text{ TeV}) t_{pp,\gamma} \sim 1.3 \times 10^{50} d_{10\text{kpc}}^2 (n_{\text{ISM}}/1 \text{ cm}^{-3})^{-1} \text{ erg}, \quad (12)$$

or the total CR proton energy

$$W_{\text{cr},p} = W_{\text{cr},p}(E_p > 1 \text{ GeV}) \sim (1 \text{ GeV}/10 \text{ TeV})^{2-\Gamma_{\text{cr},p}} \times W_{\text{cr},p}(E_p > 10 \text{ TeV}) \sim 1.9 \times 10^{51} d_{10\text{kpc}}^2 (n_{\text{ISM}}/1 \text{ cm}^{-3})^{-1} \text{ erg} \quad (13)$$

for $1 \text{ GeV} < E_p < 1 \text{ PeV}$ CR bubble with power-law spectrum (2) and with the spectral index $\Gamma_{\text{cr},p}$ equal to the spectral photon index Γ , as is expected in hadronic mechanism. We use here the value $\Gamma = 2.3$ that corresponds to the average index of known Galactic VHE γ -ray sources (H. E. S. S. Collaboration et al. 2018a) and the typical distance to the sources $d = 10 \text{ kpc}$.

Similar estimate of $W_{p,\text{tot}}$ for HOTS J1907+091 flux follows from the well-known formula for the standard chemical composition of CRs and the ambient gas (Aharonian 2004) $F_{\text{ph}}(\varepsilon > 1 \text{ TeV}) \approx 0.2 \times 10^{-11} A \text{ cm}^{-2} \text{ s}^{-1}$ for $\Gamma_{\text{cr},p} = 2.3$, where A is the scaling parameter

$$A = \frac{W_{\text{cr},p}}{10^{50} \text{ erg}} \left(\frac{d}{1 \text{ kpc}} \right)^{-2} \frac{n_{\text{ISM}}}{1 \text{ cm}^{-3}}. \quad (14)$$

In the leptonic emission scenario with IC scattering of CMB radiation by SNR/SFR/PWN shock-accelerated electrons for the HOTS J1907+091 integral energy flux the necessary energy of accelerated leptons is expected to be

$$W_{\text{cr},e}(E_e > 10 \text{ TeV}) \sim 4\pi d^2 F_\varepsilon(\varepsilon > 1 \text{ TeV}) t_{\text{IC,CMB}} \sim W_{\text{cr},p}(E_p > 10 \text{ TeV}) (t_{\text{IC,CMB}}/t_{pp,\gamma}) \sim 1.3 \times 10^{47} d_{10\text{kpc}}^2 \text{ erg}, \quad (15)$$

or the total CR lepton energy

$$W_{\text{cr},e} = W_{\text{cr},e}(E_e > 1 \text{ GeV}) \sim 16 W_{\text{cr},e}(E_e > 10 \text{ TeV}) \sim 1.9 \times 10^{48} d_{10\text{kpc}}^2 \text{ erg}. \quad (16)$$

In the HE (100 MeV – 100 GeV) band the *Fermi*-LAT extended source 4FGL J1908.6+0915e, overlapping the SGR 1900+14 position, is modelled by a power-law spectrum with integral energy flux $F_\varepsilon(\varepsilon > 100 \text{ MeV}) = 2.75 \times 10^{-11} \text{ erg cm}^{-2} \text{ s}^{-1}$ and photon index $\Gamma = 2.2$ (Abdollahi et al. 2020). In the hadronic emission scenario with photon energy $\varepsilon \approx 0.1 E_p$ a requirement for the total CR proton energy

$$W_{\text{cr},p} = W_{\text{cr},p}(E_p > 1 \text{ GeV}) \sim 1.3 \times 10^{51} d_{10\text{kpc}}^2 (n_{\text{ISM}}/1 \text{ cm}^{-3})^{-1} \text{ erg} \quad (17)$$

is similar to the considered above HOTS J1907+091 case owing to an agreement of HE and VHE spectra of SGR 1900+14 (Fig. 3).

In the leptonic-CMB emission scenario the 100 MeV – 100 GeV γ -ray band corresponds to $200 \text{ GeV} \lesssim E_e \lesssim 6 \text{ TeV}$ and a requirement for the CR $E_e > 200 \text{ GeV}$ electron energy is

$$W_{\text{cr},e}(E_e > 200 \text{ GeV}) \sim 4\pi d^2 F_\varepsilon(\varepsilon > 100 \text{ MeV}) \quad (18)$$

$$\times t_{\text{IC,CMB}}(E_e = 200 \text{ GeV}) \sim 6.4 \times 10^{49} d_{10\text{kpc}}^2 \text{ erg},$$

and for the total CR electron energy we have $W_{\text{cr},e} = W_{\text{cr},e}(E_e > 1 \text{ GeV}) \sim 1.9 \times 10^{50} d_{10\text{kpc}}^2 \text{ erg}$.

The obtained estimates of the required CR energy in the observed HE – VHE sources, namely, $W_{\text{cr},p} \sim 1.3 \times 10^{51} d_{10\text{kpc}}^2 (n_{\text{ISM}}/1 \text{ cm}^{-3})^{-1} \text{ erg}$ for hadrons and $W_{\text{cr},e} \sim 1.9 \times 10^{50} d_{10\text{kpc}}^2 \text{ erg}$ for leptons correspond to a ordinary SNR/PWN case for sources at distances of 2-5 kpc, but suggest a HNR-type of energy reserve for distances over 10 kpc.

3.3 Modelling the multiband spectral energy distribution (SED) of the SGR 1900+14 region in SNR case

In SNR and SFR models of the multiband spectral energy distribution of the SGR 1900+14 neighbourhood the observed γ -ray emission consists of hadronic contribution from proton ($i = p$) and leptonic contribution from electron ($i = e$) CRs with spectrum (2) and with its parameters $E_{\text{cr},i,\text{min}}, E_{\text{cr},i,\text{max}}, N_{0,i}, E_{\text{cr},i,0}, E_{\text{cr},i,\text{cut}}, \Gamma_{\text{cr},i,1}$. Additional parameters are electron-to-proton energy ratio K_{ep} and external shell number density n_{sh} .

Shock accelerated electron CRs will contribute to the synchrotron radio to X-ray emission and also to the observed VHE γ -ray emission via IC scattering off background photons in both upstream and downstream regions. Besides the CMB component with temperature $T_{\text{CMB}} = 2.7 \text{ K}$ and energy density $w_{\text{CMB}} = 0.26 \text{ eV cm}^{-3}$ we consider an infrared (IR, $T_{\text{IR}} = 107 \text{ K}$, $w_{\text{IR}} = 1.19 \text{ eV cm}^{-3}$) and a starlight (SL, $T_{\text{SL}} = 7906 \text{ K}$, $w_{\text{SL}} = 1.92 \text{ eV cm}^{-3}$) ones as the representative values for the population of TeV PWNe in the HGPS (H. E. S. S. Collaboration et al. 2018b).

In order to explain observed by *Fermi*-LAT (extended source 4FGL J1908.6+0915e) and HESS (extended source HESS J1907+089/HOTS J1907+091) fluxes¹ we used the NAIMA package for computation of non-thermal radiation from CR populations (Zabalza 2015). NAIMA performs Markov Chain Monte Carlo (MCMC) fitting of radiative models to observed X-ray – TeV γ -ray spectra and derives the best-fit and uncertainty distributions of spectral model parameters through MCMC sampling of their likelihood distributions. In our case *Fermi*-LAT observations include only seven bins with an overall significance only 4.58σ and an analytical power-law approximation of differential flux density of 4FGL J1908.6+0915e in the 50 MeV – 1 TeV energy range. H.E.S.S. observations of HESS J1907+089/HOTS J1907+091 are of even worse quality – only the measured integral photon flux $F_{\text{ph}}(\varepsilon > 1 \text{ TeV})$ is presented, which we have analytically approximated by power-law differential flux density in 1 –

10 TeV (see Section 2.1 and Fig. 3-7 for details). Therefore as input data for NAIMA fitting we have taken fluxes and their uncertainties for twenty bins of *Fermi*-LAT analytical approximation in the 50 MeV – 1 TeV range and for twenty bins of H.E.S.S. approximation in the 1 TeV – 10 TeV range. Fitted CR spectra was taken of a power-law (PL) and an exponential cut-off power-law (ECPL) type (2) with fixed values of parameters $E_{\text{cr},i,\text{min}}, E_{\text{cr},i,\text{max}}$ and K_{ep} (only for PL spectrum) (Table 1).

Estimated best fit CR parameters and wind shell nucleon density are presented in (Table 1) and corresponding best fit spectral energy distribution – in Fig. 3-4. As it was expected from analytical estimates, the main contribution in the observed γ -ray flux corresponds to the hadronic mechanism with a typical for ordinary relatively close ($d \lesssim 5 \text{ kpc}$) SNR value of CR energy reserve, but with high – of Hypernova type – value of CR energy for distant ($d > 10 \text{ kpc}$) SNR $W_{\text{cr},p} \approx 3 \times 10^{50} d_{10\text{kpc}}^2 (n_{\text{sh}}/10 \text{ cm}^{-3})^{-1} \text{ erg}$ even for swept-up shell with enhanced density ($n_{\text{sh}} \sim 10 \text{ cm}^{-3}$). This result is weakly sensitive to the electron contribution (K_{ep}), because the main energy losses occur in the 1 – 10 GeV range. On the other hand, the contribution of electron CR may be important and even dominant in TeV band for softer (increasing $\Gamma_{\text{cr},i}$) spectra. As it follows from (8), KN depression in background radiation of temperature T starts at electron Lorentz factor $\gamma_{e,\text{KN}}$ such that $f_{\text{KN}} \lesssim 0.5$ or at IC photon energy $\varepsilon_{\text{IC,KN}} \approx 4k_B T \gamma_{e,\text{KN}} \approx 73.3 \times 10^{13} (T/T_{\text{CMB}})^{-1} \text{ eV}$. Therefore in our case contribution of IC scattering off SL photons is negligible in TeV band.

Harder spectra ($\Gamma_{\text{cr},i} \sim 2.2 - 2.4$) can explain observations without electron CR contribution, but at the cost of increasing the total CR energy. It is important to note that hadronic flux is proportional to the product $W_{\text{cr},p} n_{\text{sh}}$, i.e., we can decrease necessary total proton CR energy increasing shell density n_{sh} , but observations (non-detection of molecular cloud) put restriction $n_{\text{sh}} \lesssim 10^2 \text{ cm}^{-3}$.

Synchrotron radiation of electron CRs in radio to X-ray band is determined by the value of magnetic field in region, filled by CRs. Excluding a narrow acceleration region around shock front, magnetic field in the rarefied wind bubble and inside HNR is expected to be of order of or less than typical interstellar value $B \lesssim 3 \mu\text{G}$. Corresponding flux does not exceed existing observational limits (Fig. 3-7).

3.4 Modelling the multiband SED of the SGR 1900+14 region in PWN case

The results of the NAIMA-fitting of SED of the SGR 1900+14 neighbourhood in the PWN model for ECBPL spectrum is presented in Fig. 6, the estimated necessary leptonic CR parameters are presented in Table 1. As we can see, similarly to the SNR case, necessary leptonic CR energy reserve $W_{\text{cr},e} \approx 2.3 \times 10^{50} d_{10\text{kpc}}^2 \text{ erg}$ is typical for ordinary relatively close ($d \lesssim 5 \text{ kpc}$) PWNe, but increases by an order of magnitude – up to Hypernova-related MWN type – for distant ($d > 10 \text{ kpc}$) PWNe.

For a decreasing $\varepsilon^2 F_{\text{ph}}(\varepsilon)$ flux in sub-TeV – TeV region (a photon index $\Gamma > 2$) an effective (average) spectral index of CR electrons should be $\Gamma_{\text{cr},e,2} = 2\Gamma - 1 > 3$. In our case we observe only this post-maximum decreasing $\varepsilon^2 F_{\text{ph}}(\varepsilon)$ flux in the all γ -ray GeV – TeV region with $\Gamma \sim 2.2$ (in the GeV band) – 2.9 (in the TeV band), therefore we use for modelling

¹ As we noted earlier the HAWC source 3HWC J1907+085 corresponds to the H.E.S.S. source HESS J1907+089/HOTS J1907+091

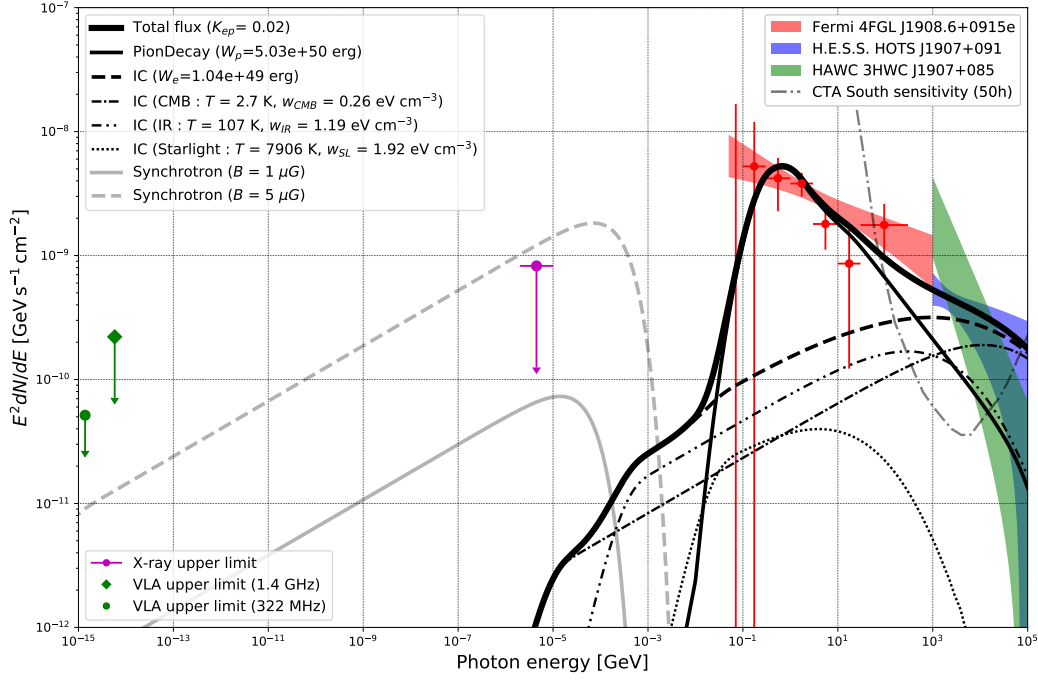


Figure 3. Modelled SED of the region of the magnetar SGR 1900+14 in SNR model. NAIMA-fitted parameters are given in Table 1 (the case of SNR at distance $d = 12.5$ kpc and shock accelerated proton and electron power-law spectra with fixed $K_{ep} = 0.02$). Observations of *Fermi*-LAT 4FGL J1908.6+0915e (in red), H.E.S.S. HOTS J1907+091 (in blue) and HAWC 3HWC J1907+085 (in green) are presented together with upper limits in the X-ray (in magenta) and the radio (in green) bands. The total γ -ray flux is a sum of hadronic (pp collisions with subsequent neutral pion decay) and leptonic (IC scattering of electrons on CMB, IR and SL background photons) contributions. Synchrotron emission is calculated for two values of the ambient magnetic field – $1 \mu\text{G}$ and $5 \mu\text{G}$. The grey dash-dotted line represents the sensitivity of the CTA South array for a zenith angle $z = 40^\circ$.

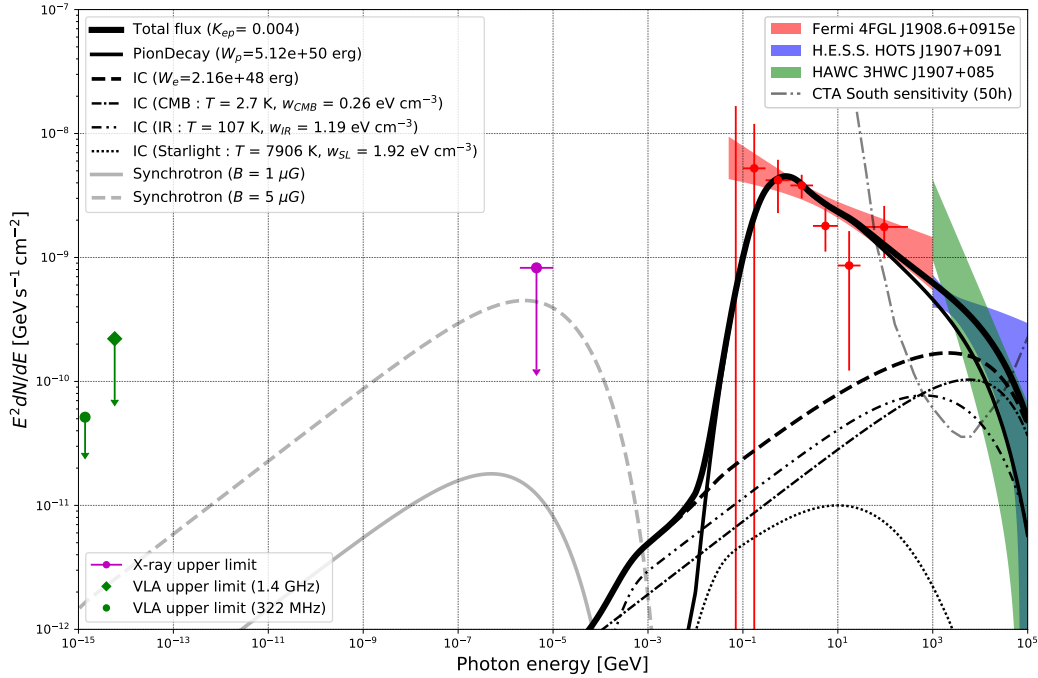


Figure 4. Same as in Fig. 3 but for exponential cut-off power-law spectra with free K_{ep} .

the PWN broad band spectrum also an inspired by "alternative model" of Ishizaki et al. (2017) ECPL electron spectrum with $E_{\min} = E_{\text{br},e} \sim 10$ GeV and $\gamma_{2,e} > 3$ in order to estimate the minimum energy of leptonic CR, necessary to explain observations. The results of the NAIMA-fitting of SED for alternative ECPL lepton spectra are presented in Fig. 6 and necessary leptonic CR parameters are presented in Table 1. Minimum leptonic CR energy reserve $\sim 6 \times 10^{49} d_{10\text{kpc}}^2$ erg is more than an order of magnitude lower than predicted in millisecond magnetar-related MWN model.

To examine a two lepton population model we consider also the case of two ($i = 1, 2$) lepton populations with power-law exponential cut-off spectra

$$N_i(E) = N_{0,i}(E/E_{0,i})^{-\gamma_{i,e}} \exp(-E/E_{\text{cut},i}), \quad (19)$$

with $\gamma_{1,e} < 2$ typical for PWN lepton CR spectra and $\gamma_{2,e} > 2$ typical for SNR electron CR spectra. SED for this case are presented in Fig. 7 and leptonic CR parameters – in Table 1. As it follows from Table 1, the explanation of TeV γ -ray emission needs six time larger electron CR energy than can be provided by external shock accelerated electron CRs with $K_{ep} = 0.02$ and cannot dominate in our case. But it still can be detected by CTA-like detectors.

4 POSSIBLE SOURCES OF HE – VHE GAMMA-RAY EMISSION FROM SGR 1900+14 REGION

4.1 Supernova Remnants

As follows from the above mentioned data, magnetar SGR 1900+14 was born about 2 kyr ago as a result of $M \approx 17M_{\odot}$ progenitor SN outburst inside the $M \sim 10^3 - 10^4 M_{\odot}$ young star cluster Cl 1900+14/SGR 1900+14.

An ordinary SNR with an explosion energy $E_{\text{SN}} \sim 10^{51}$ erg and ejected mass $M_{\text{ej}} \sim 5M_{\odot}$ in a dense ($n_{\text{mc}} = \rho_{\text{mc}}/\mu \sim 10^4 \text{ cm}^{-3}$) molecular cloud (clump) with the mean molecular weight $\mu = 1.4m_{\text{H}}$ and of radius of $R_{\text{mc}} \sim 0.5$ pc is expected to be at present at an adiabatic (Sedov - Taylor, ST) stage of evolution. The radius R_{ST}^* and age t_{ST}^* of SNR at beginning of the ST stage is determined by characteristic scales of length R_{ch} :

$$R_{\text{ST}}^* = c_1(n, s)R_{\text{ch}} = c_1(n, s)M_{\text{ej}}^{1/3}\rho_{\text{mc}}^{-1/3} = 3.1c_1(n, s)(M_{\text{ej}}/M_{\odot})^{1/3}n_{\text{mc}}^{-1/3} \text{ pc}, \quad (20)$$

and time t_{ch} :

$$t_{\text{ST}}^* = c_2(n, s)t_{\text{ch}} = c_2(n, s)E_{\text{SN}}^{-1/2}M_{\text{ej}}^{5/6}\rho_{\text{mc}}^{-1/3} = 4.2 \times 10^2 c_2(n, s)E_{\text{SN},51}^{-1/2}(M_{\text{ej}}/M_{\odot})^{5/6}n_{\text{mc}}^{-1/3} \text{ yr}, \quad (21)$$

where $c_1(n, s) \sim 1$ and $c_2(n, s) \sim 1$ are dimensionless functions of power-law density profiles of an ejecta with a power-law index n and an ambient medium with a power-law index s (Truelove & McKee 1999).

At the ST stage the time-dependent external (forward) shock wave radius R_{ST} and the velocity D_{ST} are given by

$$R_{\text{ST}}(t) = (2.026E_{\text{SN}}/\rho_{\text{mc}})^{1/5}t^{2/5} = 0.791(E_{\text{SN},51}/n_{\text{mc},4})^{1/5}t_{\text{kyr}}^{2/5} \text{ pc}, \quad (22)$$

$$\begin{aligned} D_{\text{ST}}(t) &= (2/5)R_{\text{ST}}(t)/t = (2/5)(2.026E_{\text{SN}}/\rho_{\text{mc}})^{1/2}R_{\text{ST}}(t)^{-3/2} \\ &= 2.15 \times 10^7 (E_{\text{SN},51}/n_{\text{mc},4})^{1/2}R_{\text{ST},\text{pc}}(t)^{-3/2} \text{ cm s}^{-1} \\ &= 3.07 \times 10^7 (E_{\text{SN},51}/n_{\text{mc},4})^{1/5}t_{\text{kyr}}^{-3/5} \text{ cm s}^{-1} \end{aligned} \quad (23)$$

(Truelove & McKee 1999; Reynolds 2008).

But observations do not confirm the presence of SNR inside molecular cloud. Moreover, even the molecular cloud itself is not observed. Recent modelling of star formation shows that in a young compact cluster of massive stars alike Cl 1900+14 at the moment of the first SN explosion the gas component is practically completely expelled from star cluster by stellar winds of cluster's stars and is concentrated in wind shell at ~ 40 pc. Magnetar-connected SN exploded in rarefied mix of stellar winds and, additionally energised by newborn millisecond magnetar, has reached a large size by now (see discussion in Section 4).

In our Hypernova model the HNR with $E_{\text{HNR}} \sim 10^{52}$ erg evolves inside the low-density wind bubble ($n_{\text{w}} \sim 10^{-3} \text{ cm}^{-3}$, $B_{\text{w}} \lesssim 3 \mu\text{G}$) and now ($t_{\text{HNR}} \approx 2$ kyr) is at the ST stage with the radius $R_{\text{HNR}} \approx 35$ pc and the shock velocity $V_{\text{HNR}} = 0.4R_{\text{HNR}}/t_{\text{HNR}} \approx 7 \times 10^3 \text{ km s}^{-1}$, and is approaching an extended ($R \sim 40$ pc) shell-like halo with $n_{\text{sh}} \sim 10 \text{ cm}^{-3}$ and the total swept up mass of $\sim 10^4 M_{\odot}$ (see Section 4.2 for details).

Analogously to discussed earlier SNR case, the HNR shock is also effective both proton and electron CR accelerator. For total HNR shock energy $W_{\text{HNR}} = 10^{52}$ erg we expect $W_{\text{cr},p} \sim 0.1\eta_{p,-1}W_{\text{SNR}} \sim 10^{51}\eta_{p,-1}$ erg in proton CRs and $W_{\text{cr},e} \sim 0.01K_{ep,-2}W_{\text{cr},p} \sim 10^{49}K_{ep,-2}$ erg in electron CRs.

Maximum energy of accelerated CRs with the charge Ze in the diffusive shock acceleration at the HNR shock with post-shock magnetic field $B_{\text{HNR}} = \sqrt{11}B_{\text{w}}$ according to (4) is $E_{\text{cr,max}} \approx 9Z$ PeV. For proton CRs energy losses are small during HNR age, but for electron CRs radiative cooling is important for $E_{\text{cr},e} \geq 100$ TeV.

Owing to a low density of target particles inside the HNR, we expect the main contribution to the observed VHE γ -ray emission of the SGR 1900+14 region from inelastic collisions of shock accelerated protons and heavier nuclei with target protons and heavier nuclei of dense shell-like boundary of stellar wind bubble halo with a subsequent neutral pion decay. Since the shock wave is close to the bubble boundary, but still inside the bubble $R_{\text{HNR}} \lesssim R_{\text{swb}}$, only CR from upstream shock region will effectively collide with target shell material. Their energy reserve $W_{\text{cr},p,\text{up}}$ is of order of total CR energy $W_{\text{cr},p,\text{up}} \sim W_{\text{cr},p}$ therefore in following we ignore this difference.

In considered HNR model a natural explanation for large size of young ~ 2 kyr GeV-TeV source can be given. Present radius of HNR shock $R_{\text{HNR}} \approx 35$ pc just corresponds to the size of the H.E.S.S. source HOTS J1907+091 of the angular radius $\Theta_{\text{VHE}} = 0^\circ.17 \pm 0^\circ.04$, that corresponds to the linear radius of $R_{\text{VHE}} \approx \Theta_{\text{VHE}}d_{\text{mag}} \approx 37 \pm 8.7$ pc. Hadronic component of TeV γ -ray emission is produced in the wind bubble shell of the enhanced number density n_{sh} and the radius $R_{\text{sh}} \approx 40$ pc. Accelerated at the shock front electron and proton CRs diffusively expand ahead the shock front at

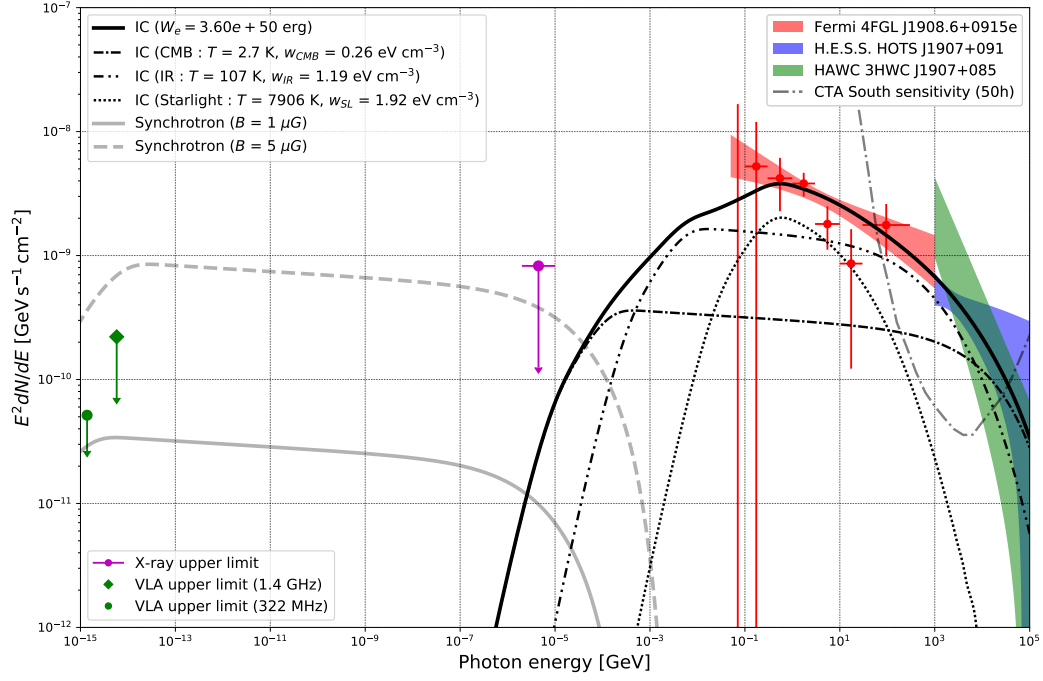


Figure 5. Modelled SED of the region of the magnetar SGR 1900+14 in PWN model. NAIMA-fitted parameters are given in Table 1 (the case of PWN at distance $d = 12.5$ kpc and termination shock/reconnection accelerated leptons with an exponential cut-off broken power-law spectrum). The total γ -ray flux is a sum of contributions from IC scattering of leptons on CMB, IR and SL background photons. The rest of the data is the same as in Fig. 3.

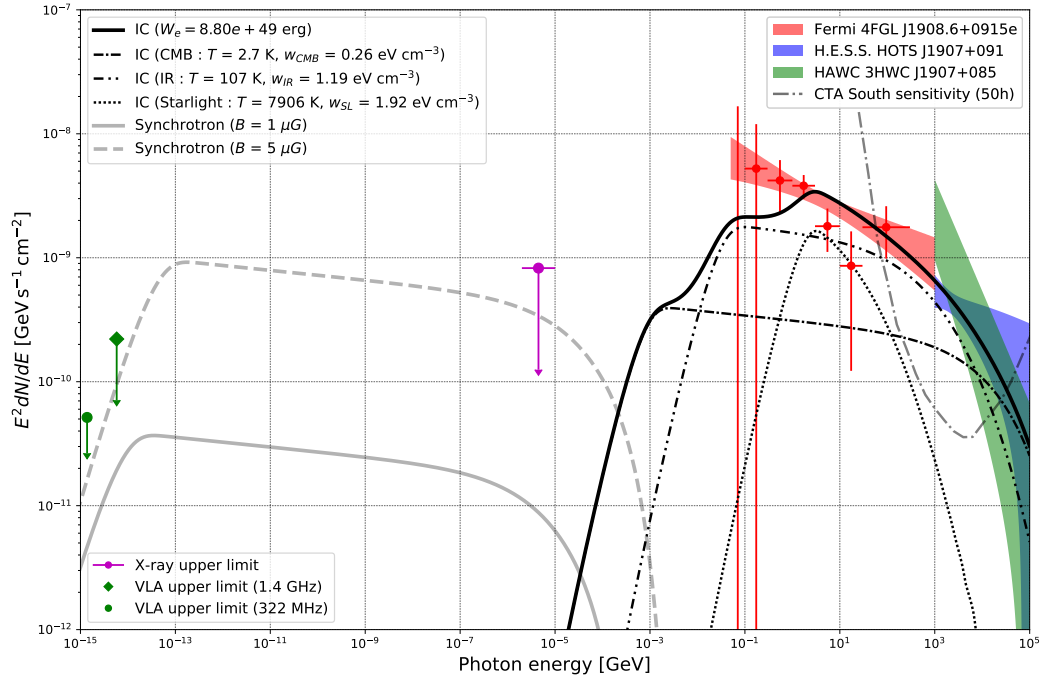


Figure 6. Same as in Fig. 5 but for alternative exponential cut-off power-law spectrum with $E_{\min} = 10$ GeV.

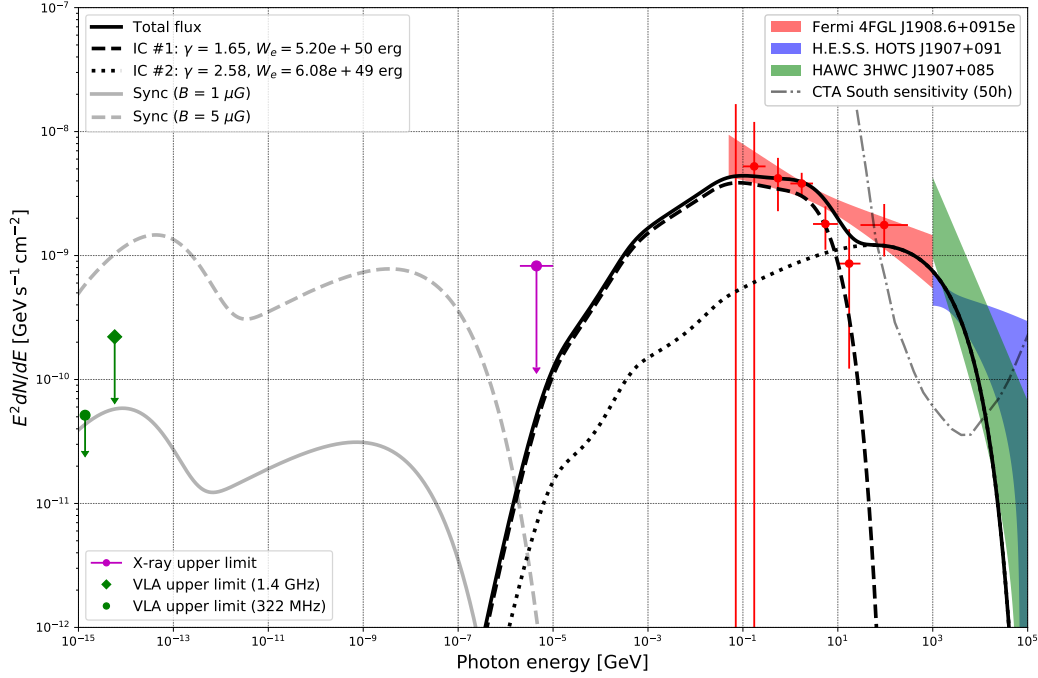


Figure 7. Same as in Fig. 5 but for two electron populations with exponential cut-off power-law spectra. For both populations only the total γ -ray fluxes as sums of contributions from IC scattering of leptons on CMB, IR and SL background photons are presented.

Table 1. SNR and PWN NAIMA-fitted models of SED from the region of the magnetar SGR 1900+14

Parameter	SNR: PL and ECPL spectra (i = p)		PWN: ECBPL and alternative ECPL spectra (i = e)		PWN: Two electron population spectra (i = e)	
	PL	ECPL	ECBPL	ECPL	ECPL #1	ECPL #2
$E_{cr,i,min}$ [GeV](fixed)	1	1	1	10	1	1
$E_{cr,i,max}$ [GeV](fixed)	1e6	1e6	1e6	1e6	1e6	1e6
$N_{0,i}$ [1/ eV]	$(1.18 \pm 0.04)e35$	$(1.42 \pm 0.05)e37$	$(1.90 \pm 0.12)e40$	$(8.91 \pm 0.50)e37$	$(4.41 \pm 0.51)e38$	$(8.81 \pm 0.44)e34$
$E_{cr,i,0}$ [TeV]	3.93 ± 0.1	0.78 ± 0.01	0.19 ± 0.01	0.175 ± 0.003	1.91 ± 0.19	1.81 ± 0.19
$E_{cr,i,br}$ [TeV]	-	-	0.0047 ± 0.0003	-	-	-
$E_{cr,i,cut}$ [TeV]	-	185.2 ± 9.5	396.7 ± 41.7	424.3 ± 21.1	0.0096 ± 0.0008	9.99 ± 1.06
$\Gamma_{cr,i,1}$	2.55 ± 0.01	2.41 ± 0.03	1.49 ± 0.07	-	1.65 ± 0.11	-
$\Gamma_{cr,i,2}$	-	-	3.04 ± 0.06	3.08 ± 0.03	-	2.58 ± 0.17
W_p [erg] (calculated [†])	$5.03e50$	$5.12e50$	-	-	-	-
W_e [erg] (calculated [†])	$1.04e49$	$2.16e48$	$3.60e50$	$8.80e49$	$5.20e50$	$6.08e49$
n_{sh} [cm ⁻³]	11.42 ± 0.66	9.81 ± 0.35	-	-	-	-
K_{ep}	0.02 (fixed)	0.0041 ± 0.0002	-	-	-	-
χ^2/ndf^*	42.10/36	30.74/34	16.54/34	40.24/36		36.64/32

* Best fit of 20 bins of *Fermi*-LAT PL 0.05-1000 GeV spectrum and 20 bins of HOTS PL 1-10 TeV spectrum approximation

[†] for distance to the source $d = 12.5$ kpc

a characteristic distance (Aharonian 2004):

$$L_{dif} \approx 2(D \times t)^{1/2} \approx 35 \left(\frac{E_{cr}}{10Z \text{ GeV}} \times \frac{3\mu G}{B} \right)^{0.24} t_{kyr}^{1/2} \text{ pc}, \quad (24)$$

where the best fitted diffusion coefficient D is taken from the Galactic diffusion-reacceleration-convection model (Yuan et al. 2017) and complemented by dependence on magnetic field in source B (Berezinskii et al. 1990)

$$D = D_0 \left(\frac{\mathcal{R}}{4 \text{ GV}} \cdot \frac{3\mu G}{B} \right)^\delta, \quad (25)$$

with $D_0 = 6.14 \times 10^{28} \text{ cm}^2 \text{ s}^{-1}$, $\delta = 0.48$, and with the slope of the injection spectrum $\Gamma_{p,e} = 2.37$ for CR rigidity $\mathcal{R} = E_{cr}/Ze > 16 \text{ GV}$ ($E_{cr} > 16Z \text{ GeV}$).

Eq.(24) implies that diffusion of electron and proton CRs in upstream region is efficient and proton CRs can penetrate in wind bubble shell and produce hadronic γ -ray emission even in case of tens-fold enhanced value of magnetic field B in shock outskirts.

Explanation of a larger size of extended *Fermi*-LAT HE γ -ray source 4FGL J1908.6+0915e modelled by disc with the angular radius of $\Theta_{HE} = 0^\circ.6$ or linear radius of $R_{HE} \approx$

$\Theta_{\text{HED}_{\text{mag}}} \approx 130$ pc is more problematic. Only proton and electron CRs with energies $E_{\text{cr}} \gtrsim 500$ GeV can reach such a distance in $t_{\text{HNR}} \approx 2$ kyr. Taking into account mentioned above low overall detection significance of this extended source (4.58σ), its large size may be a result of superposition of $\Theta_{\text{VHE}} = 0^\circ.17$ source around the magnetar and mentioned above source 4FGL J1910.2+0904c around star forming region W49A.

4.2 Star formation regions

As mentioned above, two SFRs – Cl 1900+14 and W49A – can be potential contributors to the observed γ -ray emission from SGR 1900+14 region. But quantitative analysis of expected γ -ray fluxes from these sources suggests the negligible level of their contributions. In young magnetar SGR 1900+14-connected star cluster Cl 1900+14 with only two luminosity-dominated M5 Red Supergiant (RSG) stars with masses $M \sim 14 - 18M_\odot$ and with most likely the only SN outburst of progenitor of similar mass (see discussion in Section 2.3) we do not expect the presence of powerful CR accelerated shocks besides SNR one. SFR W49A, contrary to the Cl 1900+14 case, is the most luminous Galactic SFR at similar distance of ~ 11 kpc in one of the most massive giant molecular cloud complex W49 with $M_{\text{gas}} \sim 10^6 M_\odot$ (Galván-Madrid et al. 2013, and references therein). But H.E.S.S. observations of W49A detected γ -ray emission only with the primary analysis, whereas the additional cross-check analysis does not confirmed detection level (above 5σ) (H. E. S. S. Collaboration et al. 2018d). Detection of the γ -ray emission around W49A, based on *Fermi*-LAT Pass 8 data is claimed in Xin & Guo (2021).

4.3 Pulsar wind nebulae

There are no active pulsars in the SGR1900+14 region and only a magnetar-connected relic MWN is a putative source.

Above we considered the γ -ray emission of HNR, energised by the spin-down luminosity $L_{\text{sd}} \sim 10^{48}$ erg s $^{-1}$ of the newborn millisecond magnetar with the initial spin-down time-scale $t_{\text{sd}} \sim 10^4$ s. Total released energy $E_{\text{sd}} \sim 10^{52}$ erg in the form of the non-collimated relativistic magnetar wind is transformed in energy of electron-positron pairs, accelerated at the termination shock and collected in MWN inside the expanding SN ejecta. Adiabatic expansion of MWN results in an additional acceleration of SN ejecta to a Hypernova signatures at the expense of MWN cooling $E_{\text{MWN}} \propto R_{\text{HNR}}^{-1}$ for several weeks.

But if the magnetar wind is well-collimated and jet-like (Bucciantini et al. 2007; Corsi & Lazzati 2021), it can drill the expanding ejecta and produce a long gamma-ray burst (LGRB) and a Type I superluminous SN (SLSN I) (Arons 2003; Murase et al. 2009; Piran et al. 2019). In this case the main part of magnetar rotational energy will be deposited in the relativistic Poynting-flux dominated jet with the initial Lorentz factor $\Gamma_{\text{j,ini}}(r) \gg 1$, the initial magnetization parameter $\sigma_{\text{j,ini}}(r) = B^2/4\pi\rho c^2 \gg 1$ and the isotropic luminosity

$$L_{\text{j}}^{\text{iso}} \approx L_{\text{sd}}\omega^{-1} \approx 4\pi r^2 \rho c^3 \gamma_{\text{j,ini}}^2 (1 + \sigma_{\text{j,ini}}), \quad (26)$$

where $\rho = n_l m_e$ is the lepton rest mass density (all B , σ_{j}

and ρ in the comoving frame), $\omega = \theta_j^2/4$ is the isotropic correction, θ_j is the jet half-opening angle, $t_j = t_{\text{sd}}$ and $\Delta = ct_j$ are the duration and the length of jet, correspondingly. Interaction of the jet with ISM is analogous to the case of the GRB jet (Piran 1999), only in our case the matter of the jet consists dominantly of leptons, whereas matter of the jet in a classical fireball model consists of baryons (protons) and electrons. According to the fireball model, a jet with isotropic energy $E^{\text{iso}} = L_{\text{j}}^{\text{iso}} t_j = \omega^{-1} E_{\text{rot}}$ interact with ISM and creates a jet-like analog of MWN. It includes undisturbed ISM (region 1) with the baryon (proton) number density n_1 , shocked by relativistic external shock region 2 with the proton number density n_2 , shocked by relativistic reverse shock region 3 (MWN) with the lepton number density $n_{l,3}$ (the equivalent proton number density $n_3 = (m_e/m_p)n_{l,3}$ and the undisturbed jet region 4 (the free magnetar wind) with the lepton number density $n_{l,4}$ (the equivalent proton number density $n_4 = (m_e/m_p)n_{l,4}$ (all number densities are given in comoving frames).

Dynamical evolution of the jet is described in detail in Section 4.4. Here we use numerical values of parameters presented there for fiducial values of determinative parameters: the spin down energy $E_{\text{sd}} = 10^{52}$ erg, the ISM (stellar wind) number density $n_w = n_1 = 10^{-3}$ cm $^{-3}$, the Lorentz factor of magnetar wind jet $\gamma_j = 10^3$, the jet duration $t_j = t_{\text{sd}} = 10^4$ s, the isotropic correction $\omega = 10^{-3}$ (all values are given in the centre of explosion (COE) frame), the fraction of magnetic energy in MWN $\epsilon_B = 10^{-3}$, and the comoving magnetic field in MWN $B_3 = 2 \times 10^{-2}$ G.

Reverse shock reaches the inner boundary of the jet-like magnetar wind with fiducial parameters penetrates at a distance from COE $R_\Delta = 6.5 \times 10^{18}$ cm at a moment of time $t_\Delta = R_\Delta/c = 3.2 \times 10^8$ s. For this time, the all magnetar wind leptonic plasma has crossed TS and became the MWN plasma. Both swept up and shocked by external shock ISM (region 2) and separated by contact discontinuity MWN (region 3) move with the Lorentz factor $\gamma_2 = \gamma_3 \sim f^{1/4} \gamma_j^{1/2} / \sqrt{2} \sim 5.8 \times 10^1$. On the other hand, the Lorentz factor of the MWN plasma with respect to the undisturbed magnetar wind is $\tilde{\gamma}_3 = f^{-1/4} \gamma_j^{1/2} / \sqrt{2} \sim 8.6$, that corresponds to the TS Lorentz factor $\gamma_{\text{TS}} = \sqrt{2} \tilde{\gamma}_3 \sim 1.2 \times 10^1$. All process of MWN formation up to the moment when all magnetar wind lepton plasma crosses the TS and fill in MWN is accompanied by an electron-positron CR acceleration at TS. Similarly to the ordinary PWN case, practically all magnetar wind kinetic energy is transformed to accelerated particles with the post-shock comoving energy density $w = w_e + w_B$ as a sum of the electron $w_e = \epsilon_e w$ and the magnetic field $w_B = \epsilon_B w$ energy density, where $\epsilon_e \simeq 1$ and $\epsilon_B \ll 1$ are the fractions of electron and magnetic field energy density, correspondingly. In our case the energy densities in regions 3 and 2 are equal and $w_3 = w_{e,3} + w_{B,3} = w_2 = 4\gamma_2 n_1 m_p c^2 \sim 2.0 \times 10^{-2}$ erg cm $^{-3}$ with a small admix of the magnetic field energy density $\epsilon_{B,3} \sim 10^{-3}$ for $B_3 = 2 \times 10^{-2}$ G.

At the end of MWN formation the comoving radial size of MWN was of $\Delta_3 \sim 8.5 \times 10^{15}$ cm, the transverse radius of $R_\Delta \theta_j \sim 4 \times 10^{17}$ cm, the comoving volume $V_3 = \pi \Delta (R_\Delta \theta_j)^2 \sim 4.3 \times 10^{51}$ cm, and the comoving age $t_3 \sim 3\Delta_3/c \sim 8.5 \times 10^5$ s. Maximum energy of accelerated CRs is determined by balance of the acceleration and synchrotron energy loss times and is equal to $E_{\text{cr,e,max}} = 4.4 \times 10^{14}$ eV. Energy spectrum

of accelerated CR is expected to be analogous to the mentioned above typical PWN case, i.e., exponential cut-off broken power-law one (6). Minimum energy of electrons that radiate in fast cooling regime when the energy loss time is equal to the comoving age is $E_{\text{cr},e,\text{fc}} \sim 1$ TeV. Total MWN energy reserve in the comoving frame $W_{3,\text{tot}} \sim w_3 V_3 \sim 8.6 \times 10^{49}$ erg is similar to the energy reserve of shocked ISM (region 2). In the COE frame the total energy of regions 2 and 3 are also similar and equal to $W_3^{\text{obs}} \sim W_2^{\text{obs}} \sim \gamma_3 W_{3,\text{tot}} \sim E_{\text{rot}}/4$ in each of the two jets, as expected from the energy conservation law.

To summarise, as it looks for observer in the COE frame, about 1.3×10^7 s after launch the jet-like magnetar wind pulse with the duration of $\sim 10^4$ s, traveling the distance $\sim 4 \times 10^{17}$ cm, is completely decelerated due to interaction with ISM, transferring its energy to the two-layer structure: shocked and accelerated by external shock ISM and shocked and decelerated by reverse TS magnetar wind plasma, i.e., MWN. In each jet MWN consist of accelerated leptonic CRs with the comoving energy reserve $\sim E_{\text{rot}}/4\gamma_3 \sim 4 \times 10^{49}$ erg and as a whole moves with the Lorentz factor $\gamma_3 \sim 57$. Layer of accelerated ISM has similar energy and Lorentz factor. After the mentioned above time, when the reverse shock reaches the inner boundary of the jet, the magnetar wind pressure vanishes and MWN enters the stage of free expansion in vacuum and CRs of MWN freely spread without adiabatic losses and diffusively feel a magnetar outskirts. Their mean energy increases in $\sim \gamma_3 \sim 57$ times in the COE frame. Therefore we can expect now in magnetar outskirts presence of these MWN-born leptonic CR bubble with a typical for PWN ECBPL spectrum, total energy $\sim 0.5E_{\text{rot}}$ from the both jets and a radius of ~ 40 pc according to (24). We can compare these predictions with parameters of CRs needed for explanation of γ -ray emission from SGR1900+14 outskirts in the MWN model.

It is important to note that obtained above estimates of CR parameters are rather upper limits because they correspond to the minimum energy losses of leptonic CRs in MWN.

About a half of energy, deposited by jets in the ISM and stored in thermal and kinetic energy of mentioned above layers of shocked ISM, will support further a collimated jet-like baryonic plasma flow with a decreasing Lorentz factor γ_2 until $\gamma_2 \theta_j \gtrsim 1$, and after that the jet losses a collimation and the flow starts to spherize and at a distance of order of $l_{\text{Sed}} \sim 2 \times 10^{20}$ cm enters the Sedov stage according to Eq. (22)–(23). At present, the non-relativistic jet-created shock (JCS) has parameters, similar to the previous HNR case, but with the something smaller energy $E_{\text{JCS}} \sim E_{\text{rot}}/2$ (contributions of the both jets are combined), the shock radius $R_{\text{JCS}} \approx 30$ pc and the velocity $V_{\text{JCS}} \approx 6 \times 10^3$ kms $^{-1}$. In this case we expect $W_{\text{cr},p} \sim 5 \times 10^{50} \eta_{p,-1}$ erg in proton CRs and $W_{\text{cr},e} \sim 5 \times 10^{48} \eta_{p,-1} K_{ep,-2}$ erg in electron CRs.

It is worth note, that contrary to the classical PWN scenario of HE-VHE emission generation, where only accelerated leptonic CRs produce γ -ray emission, in our case of the MWN scenario together with accelerated in MWN leptonic CRs we inevitably get also proton and electron CRs accelerated at an external shock created by magnetar wind jet. Therefore, the leptonic scenario in the MWN case includes contributions from the two lepton populations – of the MWN leptons (electron-positron pairs) and of the external shock accelerated ISM electrons (Eq.19).

To summarise, in the PWN model the observational data can be explained only when the total energy of radiating electrons is $W_{e,\text{tot}} \approx (1-5) \times 10^{50} d_{10\text{kpc}}^2$ ergs. Such energy considerably exceeds the expected CR energy in the case of ordinary distant PWNe, but it can be provided by a newborn magnetar with a millisecond period of rotation (Table 1). Like the case of HNR model, for the magnetic field inside the stellar wind bubble $B_w \lesssim 2\mu\text{G}$ the synchrotron emission does not disturb radio band upper limits (Fig. 5-7).

4.4 Source confusion

For the γ -ray sources in the Galactic plane a source confusion is a notable problem, especially for extended sources. Among the 47 unidentified HGPS sources 36 have signatures of source confusion (Devin et al. 2021)

One of the source confusion reason in the SGR 1900+14 region may be connected with TeV halos. Recent observations of TeV halos around some middle-age pulsars (Linden et al. 2017; Sudoh et al. 2019, and references therein) can be explained as IC emission of high energy electrons and positrons, accelerated at the pulsar wind TSs, but diffusively penetrated outside the PWNe at the distances ~ 10 -30 pc and interacting with the background radiation fields. TeV halos are expected to occur frequently, from 10-50 TeV halos amount detected unidentified sources and PWN candidates up to sim 50–240 TeV halos in future HAWC and CTA observations (Sudoh et al. 2019)

In ATNF Pulsar Catalogue (Manchester et al. 2005) among of middle-age (40-500 kyr) pulsars in a circle of radius $0^\circ.5$ degree around HESS J1907+089 position there are PSR J1907+0918 and PSR J1908+0909, whereas in a circle of radius 1° there are additionally PSR J1903+0925, PSR J1908+0909, and PSR J1909+0912, as well as 15 pulsars of unknown ages from The FAST Galactic Plane Pulsar Snapshot survey (Han et al. 2021). It is worth note that a full population of middle-age pulsars, including “invisible” ones with misaligned beaming angles, is about four times numerous (Linden et al. 2017). It is possible that nearby ($\lesssim 1$ kpc in order to avoid an energy crisis) invisible pulsars with TeV halos contribute to or even dominate in observed TeV flux.

γ -ray fluxes and spectra of detected sources towards the SGR 1900+14 region in Fermi Large Area Telescope Fourth Source Catalog (Abdollahi et al. 2020), especially the extended source 4FGL J1908.6+0915e can be biased by the source confusion as well. This extended source is overlapping with the SGR 1900+14 and the SNR G42.8+0.6. But, as mentioned above, this SNR is detected only as a weak radio source without any another non-thermal activity and is unlikely to be able to generate a notable γ -ray emission. There are also three unidentified 4FGL sources in this region: J1908.7+0812, J1910.2+0904c, and J1911.0+0905 (sources 1, 2, and 3 in Fig. 1, correspondingly). 4FGL J1910.2+0904c has a flag 5 as an alert to confusion and an append c (coincident with an interstellar clump) and is very likely physically connected with the SFR W49A (Xin & Guo 2021). The SFR W49A includes a lot of young massive stars and HII regions embedded in a dense molecular cloud with promising conditions for γ -ray emission of stellar wind shock accelerated CRs, but without signatures of SNRs. Potentially, it could contribute to the γ -ray emission from a western hemisphere of an extended source 4FGL J1908.6+0915e (Fig. 3 in

Li et al. (2017)). 4FGL J1911.0+0905 is associated with the SNR W49B (G043.3-00.2), known as the TeV source HESS J1911+090 (H. E. S. S. Collaboration et al. 2018a), but due to a point-like type and considerable spacing we do not expect a severe source confusion with the SGR 1900+14 region.

5 COMPREHENSIVE ANALYSIS OF THE HYPERNOVA MODEL

We have shown that gross characteristics of the observed HE and VHE γ -ray emission from the region of the SGR 1900+14 together with the absence of detectable emission in lower energy bands can be explained in the framework of the Hypernova-like explosion of a SGR 1900+14 progenitor massive star with the dominant contribution of the newborn fast rotating magnetar in the SN energy reserve. The main requirement for a successful model is a high amount of an energy deposited in accelerated hadrons and leptons in both cases of the γ -ray emission generation: by the dominant contribution of the hadronic mechanism in the HNR model (the necessary total energy of the hadronic CR component is $W_{\text{cr},p} \sim 5 \times 10^{50}$ erg) or by the leptonic mechanism in the MWN model ($W_{\text{cr},e} \sim 5 \times 10^{50}$ erg) (Table 1).

There are observational and theoretical arguments supporting an evolution scenario with the SGR 1900+14 progenitor as a Hypernova/Supernovae (SLSN).

5.1 Hypernova signatures in the optical band

The magnetar SGR 1900+14 agrees in a sky position, a distance, and an age with the 4 BCE "po star" – the visible by naked eye (~ 5 mag) transient (~ 1 month) immovable source – from ancient Chinese record dated 4 BC Apr 24 (Wang et al. 2002; Stephenson & Green 2005). Indeed, for the mentioned above distance $d_{\text{mag}} = 12.5 \pm 1.7$ kpc and the visual extinction $A_V = 12.9 \pm 0.5$ mag (Davies et al. 2009) this explosion would have been optically observable only when the absolute magnitude of Hypernova near to the maximum light was $M = m + 5 - 5 \log(d_{\text{mag}}/\text{pc}) - A_V \approx -23$ mag. Estimated value of M is slightly more than in the case of the most luminous SN yet found ASASSN-15lh (SN 2015L) with $M_{\text{AB}} = -23.5 \pm 0.1$ mag (Dong et al. 2016) and is similar to $M \gtrsim -23$ mag SLSNe cases (Moriya et al. 2018; Angus et al. 2019). Even for a more conservative estimate $A_V = N_{\text{H}} / ((2.04 \pm 0.05) \times 10^{21} \text{ cm}^{-2})$ for the first Galactic quadrant (Zhu et al. 2017), so that $A_V = 9.3$ mag from X-ray band suggested value $N_{\text{H}} = 1.9 \times 10^{22} \text{ cm}^{-2}$, the absolute magnitude of the SGR 1900+14 progenitor $M \approx -19.4$ mag is noticeably lower than the typical value for core collapse SNe. An improved SGR 1900+14 age estimate $\tau_c \approx 2.4$ kyr from new P and \dot{P} data (Tamba et al. 2019) agrees with the "po star" age, taking into account an uncertainty of spin-down rate \dot{P} determination (Tamba et al. 2019).

5.2 Hypernova remnant formation

The second argument, supporting Hypernova nature of the SGR 1900+14 progenitor, is an absence of SNR signatures in radio to X-ray band. Vrba et al. (2000) have classified this cluster as embedded in parental molecular cloud, but Morales et al. (2013) did not find signatures of a molecular

cloud (clump) as a dominated by mass component of the star cluster Cl1900+14/SGR 1900+14 (see subsection 2.2 for details).

Molecular clumps are destroyed by a newly formed star backreaction even before a SN era (see discussion in Krumholz et al. 2019; Dinnbier & Walch 2020). Limongi & Chieffi (2018) showed that rotating ($V = 300 \text{ km s}^{-1}$) massive ($M = 15 M_{\odot}$) star with solar metallicity ($[\text{Fe}/\text{H}] = 0$)² evolves to a Wolf-Rayet (WR) evolution stage with a lifetime $t_{\text{WR}} \approx 3.68 \times 10^5 \text{ yr}$ and a total WR wind mass loss $M_{\text{w,He}} \approx 4.0 M_{\odot}$ of helium.

At the WR stage, for the typical WR wind with the mass-loss rate $\dot{M}_{\text{w}} \sim 10^{-5} M_{\odot} \text{ yr}^{-1}$, the wind velocity $V_{\text{w}} \sim 10^8 \text{ cm s}^{-1}$ and the mechanical luminosity $L_{\text{w}} = 0.5 \dot{M}_{\text{w}} V_{\text{w}}^2$ the expected WR wind bubble radius R_{bub} at the time t_{w} since the beginning of WR stage is (Weaver et al. 1977):

$$R_{\text{bub}} = \left(\frac{125}{154\pi} \frac{L_{\text{w}}}{\rho_{\text{cl}}} \right)^{1/5} t_{\text{w}}^{3/5} \quad (27)$$

$$= 8.6 \times 10^{-2} \dot{M}_{\text{w},-5}^{1/5} V_{\text{w},8}^{2/5} n_{\text{cl},4}^{-1/5} t_{\text{w,kyr}}^{3/5} \text{ pc}.$$

In our case the WR wind destroys parental molecular cloud when $R_{\text{bub}} \approx R_{\text{cl}} \approx 0.7 \text{ pc}$ at time moment $t_{\text{w}} = 33 \text{ kyr}$, that is, shorter of the WR stage lifetime $t_{\text{w}} \ll t_{\text{WR}} = 368 \text{ kyr}$. It means that the WR wind alone can destroy a molecular clump in $\sim 30 \text{ kyr}$, even before the first SN explosion. Till the moment of the first SN outburst, joint action of stellar winds of three $M \sim 14 - 18 M_{\odot}$ stars in the newborn SGR 1900+14 star cluster can blow-up the gas component of the parent $M_{\text{cl}} \sim 10^3 M_{\odot}$ clump up to $\sim 40 \text{ pc}$, forming an extended ($\sim 10 - 20 \text{ pc}$) shell-like halo of fragmented debris of wind bubble shells with the mean number density $n_{\text{sh}} \sim 10 \text{ cm}^{-3}$ and the total cluster plus ISM ($n_{\text{ISM}} \sim 1 \text{ cm}^{-3}$) swept mass $\sim 10^4 M_{\odot}$ (van Marle & Keppens 2012; Geen et al. 2015; He et al. 2019; Dinnbier & Walch 2020).

In the Hypernova case, the gas component of ejecta (with-out of $2 M_{\odot}$ of dust shell) of $M_{\text{ej}} \sim 3 M_{\odot}$ will be accelerated by a newborn magnetar with a rotation energy $E_{\text{rot}} \sim 10^{52} \text{ erg}$ up to the velocity $V_{\text{ej}} \sim (2E_{\text{rot}}/M_{\text{ej}})^{1/2} \sim 1.9 \times 10^9 \text{ cm s}^{-1}$ (Woosley 2010; Suzuki & Maeda 2019). Accelerated ejecta will expand in a mix of $n_{\text{w}} \sim 10^{-3} \text{ cm}^{-3}$ winds from the exploded WR-star and the still present in the star cluster two RSG and a few BSG stars (Davies et al. 2009). For a constant ejecta density profile (with power-law index $n = 0$) and a constant density of bubble interior (with power-law index $s = 0$), HNR enters the ST stage at the distance $R_{\text{ST}}^* \approx 32 \text{ pc}$ at the moment of time $t_{\text{ST}}^* \approx 1.6 \text{ kyr}$ and reaches in the ST regime $R_{\text{ST}} \approx 35 \text{ pc}$ at the present time $t_{\text{SNR}} \approx 2 \text{ kyr}$.

5.3 Infrared emission of the clumpy Hypernova ejecta

Acceleration of an ejecta shell by a magnetar wind is accompanied by the development of the Rayleigh-Taylor instability at a wind bubble-ejecta boundary, which can considerably complicate the process of shell acceleration (Blondin & Chevalier 2017). Recent 3D-modelling of an initial interaction of a powerful MWN ($E_{\text{MWN}} \approx E_{\text{rot}} \sim 10^{52} \text{ erg}$) with

² As we mentioned above, such a model provides an observed dust mass $M_{\text{dust}} \gtrsim 2 M_{\odot}$ in the SGR 1900+14 IR shell.

a typical SN ejecta ($E_{\text{ej}} \sim 10^{51}$ erg), presented in [Suzuki & Maeda \(2019\)](#), shows that considerable wind energy dominance results in the Rayleigh-Taylor instability of the MWN surface.

In our case of $L_{\text{sd}} = 10^{48}$ erg s $^{-1}$ and $t_{\text{sd}} = 10^4$ s MWN with the time-dependent radius $R_{\text{MWN}} \approx 2 \times 10^{11} (t/t_{\text{sd}})^{5/4}$ cm is deep inside the exploding star.

The relativistic MWN plasma mixes with the SN ejecta and destroys a regular shell-like structure of the ejecta. Numerous relativistic jet-like MWN plasma flows penetrate a steep gradient of ejecta layers and accelerate an external ejecta layers by mildly relativistic forward shock.

This escaping through ejecta channels plasma carries out a dominant part of a magnetar wind energy, living a dense clumpy part of an ejecta with a relatively low energy gain. In the case of considered in [Suzuki & Maeda \(2019\)](#) ejecta of $M_{\text{ej}} = 10 M_{\odot}$ this clumpy part of ejecta with a mass $M_{\text{cl}} \approx 0.5 M_{\text{ej}}$ reaches a typical velocity of $\sim 0.01c$ and for the SNR age of 2 kyr will be at distance of ~ 6 pc from the outburst place. In our case of the $M_{\text{ej}} \approx 5 M_{\odot}$ ejecta, a fragmentation of the ejecta is expected earlier and with lower debris velocities in accordance with the observed SGR 1900+14 IR shell radius of ~ 2 pc.

The discussed in subsection 2.2 elliptical fit to the IR ring with ratio of axes $\approx 2 : 1$ ([Wachter et al. 2008](#); [Natale et al. 2017](#)) We propose another model of IR morphology, where observed IR ring of radius $R_{\text{ring}} \approx 27'' \approx 1.7$ pc consists of a newly formed dust in the Hypernova ejecta and is centred on the position of the magnetar's birthplace about 2 kyr ago (Fig. 2). The newborn magnetar with the transverse velocity $V_t = 130$ km s $^{-1}$ needs just 2 kyr for traveling the distance of $5''$ or 0.3 pc from its birthplace to the present position. In our model only dust-free cavity in the inflated part of ring was produced by the *anisotropic* giant flare in August 1998 (or during the possible previous, even more energetic, giant flare). A short flare duration ($\lesssim 1$ s) in comparison with the magnetar's rotational period ($P = 5.2$ s) results in an anisotropic energy release with a collimation angle ~ 1 rad in an agreement with observations. Observed dust mass $M_{\text{dust,out}} \sim 2 M_{\odot}$ can also be explained in star evolution models. [Marassi et al. \(2019\)](#) shown, that evolution of a rotating ($V_{\text{rot}} = 300$ km s $^{-1}$) calibrated (fixed) energy star model with an initial mass $M_{\text{ini}} = 15 M_{\odot}$ and solar metallicity ([Fe/H]=0) ends by a pre-SN mass of $M_{\text{preSN}} = 6.22(6.22) M_{\odot}$ and a 1b SN outburst with an explosion energy $E_{\text{SN}} = 0.93(1.2) \times 10^{51}$ erg, an ejected mass of $M_{\text{ej}} = 4.23(5.21) M_{\odot}$ and dust mass of $M_{\text{dust}} = 1.5(2.25) M_{\odot}$. An additional energy supply from a newborn magnetar with a rotational energy $E_{\text{rot}} \approx 2 \times 10^{52} P_{i,-3}^{-2}$ erg will provide a Hypernova type of an explosion ([Murase et al. 2015](#); [Kashiyama et al. 2016](#); [Metzger et al. 2018](#); [Piran et al. 2019](#)).

5.4 Magnetar wind nebula formation in a collimated jet-like magnetar wind

Relativistic outflow from a magnetar in the form of a collimated jet is expected in magnetar-related Hypernovae with possible long GRBs ([Arons 2003](#); [Murase et al. 2009](#); [Piran et al. 2019](#)). Hydrodynamics of jet interaction with ISM is analogous to the case of GRB jet ([Piran 1999](#)).

Dynamical evolution of jet depends, first of all, on jet's en-

ergy E^{iso} . Similar to classical PWN case Poynting flux dominated jet at large distances transforms into kinetic energy dominated jet with $\sigma_j \lesssim 1$ and increased correspondingly Lorentz factor $\gamma_j \sim \gamma_{j,\text{ini}} \sigma_{j,\text{ini}}$: $E^{\text{iso}} \approx 4\pi r^2 n_{l,4} m_e c^3 \gamma_j^2 t_j$. Another important parameters are the scale of non-relativistic (Sedov stage) shock expansion

$$l_{\text{Sed}} = \left(\frac{E^{\text{iso}}}{n_1 m_p c^2} \right)^{1/3} = 1.8 \times 10^{20} \left(\frac{E_{\text{rot},52}}{\omega_{-3} n_{1,-3}} \right)^{1/3} \text{ cm}, \quad (28)$$

undisturbed jet's length $\Delta = ct_j = 3 \times 10^{14} t_{j,4}$ cm, lepton number density in jet at the distance r

$$n_{l,4}(r) = \frac{E_{\text{rot}}}{4\pi r^2 \omega \Delta \gamma_j^2 m_e c^2} = 3.3 \times 10^3 \frac{E_{\text{rot},52}}{\omega_{-3} t_{j,4} \gamma_{j,3}^2 r_{18}^2} \text{ cm}^{-3} \quad (29)$$

the distance $R_\gamma = l_{\text{Sed}} \gamma_j^{2/3}$ at which the jet starts to slow down (loses half of the initial energy) and the distance R_Δ at which reverse shock reaches the inner boundary of jet (i.e. all magnetar wind plasma penetrates the TS and formation of MWN is completed)

$$R_\Delta = (l_{\text{Sed}}^3 \Delta)^{1/4} = 6.5 \times 10^{18} \left(\frac{E_{\text{rot},52} t_{j,4}}{\omega_{-3} n_{1,-3}} \right)^{1/4} \text{ cm}. \quad (30)$$

At that distance the jet's density to ISM density ratio is

$$f = \frac{\rho_4}{\rho_1} = \frac{n_4}{n_1} = 4.2 \times 10^1 C_f \gamma_{j,3}^{-2}, \quad C_f = \left(\frac{E_{\text{rot},52}}{\omega_{-3} t_{j,4}^3 n_{1,-3}} \right)^{1/2}. \quad (31)$$

With these parameters at hand, we can estimate the physical parameters of newborn MWN at moment of time $t_\Delta = R_\Delta/c$ s. Both parts of the two-component jet – regions **2** and **3** are separated by the contact discontinuity and move with the same Lorentz factor

$$\gamma_2 = \gamma_3 = f^{1/4} \gamma_j^{1/2} / \sqrt{2} = 5.8 \times 10^1 C_f^{1/4}. \quad (32)$$

The Lorentz factor of MWN plasma with respect to the undisturbed magnetar wind is

$$\bar{\gamma}_3 = f^{-1/4} \gamma_j^{1/2} / \sqrt{2} = 8.6 C_f^{-1/4} \gamma_{j,3}, \quad (33)$$

that corresponds to the TS Lorentz factor $\gamma_{\text{TS}} = \sqrt{2} \bar{\gamma}_3$ in the free wind frame. The energy densities w are the same in both regions

$$w_2 = w_3 = 4 \gamma_2^2 n_1 m_p c^2 = 2.0 \times 10^{-2} n_{1,-3} C_f \text{ erg cm}^{-3}. \quad (34)$$

As in the case of ordinary PWN magnetic field energy density we parametrise by magnetic energy fraction $\epsilon_B = w_B/w$ with $\epsilon_B \sim 10^{-3}$. For the comoving magnetic field in MWN we obtain

$$B_3 = (8\pi \epsilon_B w_3)^{1/2} = 2 \times 10^{-2} \epsilon_{B,-3}^{1/2} n_{1,-3}^{1/2} C_f^{1/4} \text{ G}. \quad (35)$$

The comoving size of MWN is

$$\delta_3 = \Delta \gamma_j / 4 \bar{\gamma}_3 = 8.5 \times 10^{15} t_{j,4} C_f^{1/4} \text{ cm} \quad (36)$$

and the comoving MWN formation time is $t_{\text{MWN}} = 3\delta_3/c = 8.5 \times 10^5 t_{j,4} C_f^{1/4}$ s. Maximum energy of accelerated leptonic CRs can be determined from the equality of the acceleration time and the energy loss time (Eq. (11) and in our case is $E_{e,\text{max}} = 6.0 \times 10^{14} B_{3,-2}^{-1/2}$ eV. At the same time, CRs with the energy loss time smaller than the MWN age t_{MWN} or with $E_e \gtrsim 4.5 \times 10^{12} t_{j,4}^{-1} C_f^{1/4}$ eV will radiate in the fast cooling regime.

6 DISCUSSION

Above we have modelled observed γ -ray emission from the SGR 1900+14 region for both hadronic and leptonic scenarios from three classes of potential sources presented or expected in the area under consideration: SNRs (a magnetar-connected SNR, the SNR G042.6, and the SNR W49B), PWNs (a hypothetical magnetar-connected PWN and TeV halos), and SFRs (Cl 1900+14 and W49A)

All of them, although to varying degrees, can contribute to the observed γ -ray emission. But while there are several potential sources, none are without problems. It is useful to compare this region with the region around the mentioned above magnetar SGR 1806-20 (of 8.7 kpc distance) with similar GeV-TeV fluxes and morphology: the extended 4FGL J1808.2-2028e source with the radius of $\Theta_{\text{HE}} = 0^\circ.65$ (Yeung et al. 2016) is associated with the unidentified point-like HESS J1808-204 source (H. E. S. S. Collaboration et al. 2018e,a). In addition to the magnetar SGR 1806-20 itself with a possible PWN, potential sources include its host: the massive star cluster Cl* 1806-20 with four WR stars and four OB supergiants with powerful stellar winds. Once more, the hypergiant LBV 1806-20 wind powers a radio-nebula G10.0-0.3. Another promising γ -ray source towards the magnetar SGR 1806-20 region is a shell-type SNR G9.7-0.0 (of 4.7 kpc distance) interacting with a nearby MC. It is worth noting that in the 3-500 GeV band the extended morphology of 4FGL J1808.2-2028e consists of two separated clumps, coincident with HESS J1808-204 and the SNR G9.7-0.0, respectively (Yeung et al. 2016; H. E. S. S. Collaboration et al. 2018e,a, and references therein)

All these classes of potential sources are presented in the SGR 1900+14 region as well. But their abilities to provide the observed γ -ray fluxes do not look so optimistic. Magnetar's host massive star cluster Cl 1900+14 with only two M5 RSG stars and without OB or WR stars (see Section 2.3 for details) cannot ensure effective CR acceleration. The other stellar cluster - the luminous SFR W49A looks more promising, but displays only a weak point-like GeV γ -ray source (if any). Analogously to the 4FGL J1808.2-2028e case, the SFR W49A could contribute to one overlapping clump in a hypothetical two-clump structure of 4FGL J1908.6+0915e

Among the two SNRs in the SGR 1900+14 region the SNR G42.8+0.6 manifests himself only as a weak radio shell without any X-ray or γ -ray activity, whereas the SNR G043.3-00.2 (W49B) is detected as a point source in HE and VHE γ -rays, but out of the region considered.

In this situation we expect that the dominant contribution to γ -ray emission from the SGR1900+14 region most likely is provided by the magnetar-related SNR/MWN and mentioned above hypothetical TeV halos due to the source confusion.

6.1 Magnetar-connected HNR/MWN model

The magnetar-related solution with sources at the magnetar distance of 12.5 kpc requires the Hypernova-type energy reserve $\sim 10^{50} - 10^{51}$ erg in CRs in both hadronic and leptonic scenarios. In Section 4 we presented a detailed description and verified reliability of the HNR/MWN model. Hypernovae and GRB remnants have been proposed as unidentified TeV sources for a long time (Ioka & Mészáros 2010; Fox et al. 2013). A potential weakness of this model is the small

number of Hypernovae in our Galaxy. The measurement of the local core-collapse SN (CCSN) rate and of the subclass of hydrogen-free superluminous SN (SLSN-I) rate using SN rates from the Palomar Transient Factory gives the local ratio of SLSN-I to all CCSN types of $\sim 1/3500^{+2800}_{-720}$ (Frohmaier et al. 2021). For the Galactic CCSN rate $\sim 1/30 \text{ yr}^{-1}$ and a typical HNR age $\sim 10^5 \text{ yr}$ the expected number of HNRs in our Galaxy is about a few. In particular, HNRs may reside in the Galactic center (He et al. 2020) and in the Cygnus region (Fang & Murase 2021).

Generally, magnetar-connected HNR/MWN models give reasonable explanation of the set of observational multiwavelength data concerning the magnetar SGR 1900+14 and its neighbourhood. But some parameters of these model are far from their typical values. So we see the main challenge of the HNR model in the requirement of the high value of total hadronic CR energy $W_{\text{cr,p}} \sim 5 \times 10^{50} (n_{\text{sh}}/10 \text{ cm}^{-3})^{-1} \text{ erg}$ (Table 1, Figs. 3, 4).

As in the HNR case, the main challenge of the MWN model is the requirement of the high value of the total energy of accelerated leptons $W_{\text{cr,e}} \sim 5 \times 10^{50} \text{ erg}$, that is, on the order of the total energy of protons in the HNR model (Table 1, Figs. 5-7).

A newborn millisecond magnetar can help to solve the energy problem, but another challenge in the magnetar case is the low probability of magnetars' millisecond periods. Recent results concerning the parameters of magnetars, connected with the long GRBs and the Type I SLSNe suggest possible millisecond equilibrium spin period due to the fallback accretion (Lin et al. 2020).

Some fine tuning is connected with the magnetar jet and the jet-created MWN. For parameters considered leptons in the transient MWN radiate in the slow cooling regime without serious energy losses and are spread in the magnetar region with considerable part of jet energy. Therefore our estimates of the energy reserve of accelerated CRs can be considered as a lower limit.

Presented here model of the magnetar jet does not take into account a possible baryon contamination. Each baryon (proton) in the relativistic jet carries energy m_p/m_e times higher than electron. Therefore, even small admix of baryons considerably reduces the leptonic energy reserve and, correspondingly, leptonic emission. Our estimations can be considered as an upper limit on expected leptonic emission for magnetar jets.

Till now, only γ -ray emission is detected from the magnetar SGR 1900+14 outskirts. In both HNR and MWN cases the radio and X-ray non-detection corresponds to a low value of magnetic field $B \lesssim 2 \mu\text{G}$ in the magnetar neighbourhood. Such values of B are expected in a large $\gtrsim 30 \text{ pc}$ rarefied $n_w \sim 10^{-3} \text{ cm}^{-3}$ stellar wind bubbles.

6.2 Testing of alternative models

As mentioned above, a contribution from a TeV halo around a nearby (of $\sim 1 \text{ kpc}$ distance) invisible pulsar could also be an option. The contribution of other sources, including SFRs, cannot be ruled out as well. Additional multiwavelength – from radio to multi-TeV bands – and spectral observations are needed to clarify the nature of the γ -ray sources in this region.

First of all, new observations in TeV band are very promis-

ing to establish the nature of sources. Already future observations of the SGR 1900+14 region by the forthcoming Cherenkov Telescope Array (CTA, [Cherenkov Telescope Array Consortium et al. \(2019\)](#)) in the short-term programme (years 1-2) of the CTA Galactic Plane Survey by the South observatory with an equivalent exposure time 11.0 h (a point-source sensitivity 2.7 mCrab) should detect sources in the SGR 1900+14 region. The combination of high resolution imaging atmospheric Cherenkov telescopes (IACTs) H.E.S.S., CTA and wide field of view air shower arrays (ASAs) HAWC, LHAASO in forthcoming observations will reveal the spectral and morphological features of sources. In the hadronic HNR model we expect a shell-like or an arch-like morphology and a power-law $\Gamma_{\text{cr,p}} = 2.2 - 2.5$ spectrum with an exponential cut-off, whereas both leptonic MWN and TeV halo models are expected to have a filled center plerion-like morphology and a hard sub-cutoff spectrum. Once more, in the TeV halo case the spatial extent of associated SNR/X-ray PWN, if observed, is significantly larger/smaller than of the halo himself ([Linden et al. 2017](#); [Sudoh et al. 2019](#)).

The high angular resolution of the CTA and *Fermi*-LAT in multi-GeV band can help to investigate sub-structures and energy-dependent morphology of the extended *Fermi*-LAT 4FGL J1908.6+0915e source. If the two-clump structure as in the case of the magnetar SGR 1806-20 is confirmed, a hybrid model of multi-GeV γ -ray emission may be more adequate. It may include mixes of hadronic and leptonic contributions from the clump that overlaps the SFR W49A and from the magnetar - connected clump. Analysis of HE spectra of clumps can help to disentangle confused sources ([Yeung et al. 2016](#); [Cherenkov Telescope Array Consortium et al. 2019](#)).

Multi-wavelength observations in the radio to X-ray band with the high angular resolution open up additional possibilities for testing alternative models. New observations of mentioned above pulsars in the SGR 1900+14 region by FAST ([Han et al. 2021](#)) will determine their spin-down rate and thus their physical parameters as potential sources of confused TeV halos. It will also be important to look for radio-signatures of synchrotron emission from PWNe and SN remnants as well as for HI, CO, OH radio-lines due to a SNR shock-molecular cloud interaction ([Slane et al. 2015](#); [Lee et al. 2015](#)). Detection of the shock-molecular cloud interaction would allow to clarify the distance to the γ -ray source, which is of fundamental importance for the HNR model.

Promising perspective for clarifying the nature of the γ -ray sources in the SGR 1900+14 region is connected with the forthcoming extended ROentgen Survey with an Imaging Telescope Array (eROSITA) on board the Spectrum-Roentgen-Gamma (SRG) mission, that will be about 25 times more sensitive than the ROSAT All-Sky Survey in the soft X-ray (0.2 - 2.3 keV) band ([Predehl et al. 2021](#)).

7 CONCLUSIONS

We have modelled the observed HE and VHE γ -ray emission from the sky region of the magnetar SGR 1900+14 as a result of the contributions of individual sources available here, namely, the SNRs G42.8+0.6 and W49B, the SFRs Cl 1900+14 and W49A, as well as an undetected yet magnetar-

connected SNR and possible MWN. Source confusion with TeV halos is also probable.

Our main conclusions can be summarised as follows.

1. Physical conditions in the SNRs G42.8+0.6 and W49B, as well as in the SFRs Cl 1900+14 and W49A cannot provide a significant contribution to the observed HE and VHE γ -ray emission.

2. A set of observational multiwavelength data may be explained in a model of a magnetar-connected SN, exploded about 2 kyr ago at a distance of 12.5 kpc and mentioned in ancient Chinese records on 4 BC Apr 24. SN should be of Hypernova type with the explosion energy $E_{\text{HNR}} \sim 10^{52}$ erg derived from the rotational energy $E_{\text{rot}} \approx 2 \times 10^{52} P_{1.3}^{-2}$ erg of the newborn millisecond strongly magnetised X-ray pulsar - magnetar SGR 1900+14. Equilibrium millisecond period of magnetar with $B_s = 4.3 \times 10^{14}$ G is expected due to the fallback accretion.

3. The extremely high initial magnetic dipole spin-down luminosity will result in energization of the Hypernova ejecta and in formation of the MWN. Relative shares of the energy input to the Hypernova ejecta and to the MWN are model-dependent and can be estimated from the analysis of new observations.

4. In the HNR model, the energy-dominated Hypernova ejecta with $E_{\text{HNR}} \approx E_{\text{rot}} \approx 10^{52}$ erg evolves inside the low-density wind bubble creating the HNR at the ST stage at present. Shock accelerated nuclei and electrons are diffusively spread over the observed γ -ray sources and γ -ray emission is generated mainly by the hadronic mechanism (pp collisions with subsequent neutral pion decay) in the dense ($n_{\text{sh}} \sim 10 \text{ cm}^{-3}$) extended shell-like halo of swept up mass of $\sim 3 \times 10^4 M_{\odot}$. In the TeV band the contribution of the leptonic mechanism (IC scattering of background CMB, IR and SL photons by shock accelerated electrons) can be dominant.

5. The powerful relativistic collimated jet-like magnetar wind can effectively penetrate the Hypernova ejecta, producing twin GRB-like jets in a rarefied stellar wind bubble. Due to the leptonic jet deceleration, the two transient MWNe with $E_{\text{MWN}} \lesssim 0.5 E_{\text{rot}} \approx 10^{52}$ erg arise and the jet's energy is partially transferred to TS/reconnection accelerated electrons and positrons. After an jet shutdown the accelerated leptons spread over the observed γ -ray sources and γ -ray emission is generated by the leptonic mechanism.

Certainly, a more realistic model should include contributions from both hadronic and leptonic models, but sparse observational data available do not allow us to build a fully quantitative model for the γ -ray emission of the SGR 1900+14 environment.

6. The source confusion caused by expected TeV halos in the Galactic plane is actual for the region of SGR 1900+14.

In the next few years new multiwavelength observations in radio (FAST), X-ray (eROSITA), and γ -ray (MAGIC, H.E.S.S., HAWC and LHAASO) bands could clarify source characteristics and improve our understanding of the physical processes in SNRs/MWNe and the nature of the γ -ray emission from the region of the magnetar SGR 1900+14.

ACKNOWLEDGEMENTS

We are grateful to the anonymous reviewers for very attentive and helpful comments and suggestions that helped us signifi-

cantly improve the quality of the manuscript. The Spitzer IR image of the SGR 1900+14 environment is shown by courtesy NASA/JPL-Caltech.

Data availability statement: All observational data used in the paper are publicly available in the cited works. The datasets generated and analyzed during the current study are available from the corresponding author on reasonable request.

REFERENCES

- Aab A., et al., 2015, *ApJ*, **804**, 15
- Abbasi R. U., et al., 2014, *ApJ*, **790**, L21
- Abdalla H., et al., 2021, arXiv e-prints, p. arXiv:2107.01425
- Abdollahi S., et al., 2020, *ApJS*, **247**, 33
- Abeysekara A. U., et al., 2017, *ApJ*, **843**, 40
- Abeysekara A. U., et al., 2018, *Nature*, **562**, 82
- Acero F., et al., 2016, *ApJS*, **224**, 8
- Aharonian F. A., 2004, Very high energy cosmic gamma radiation: a crucial window on the extreme Universe, doi:10.1142/4657.
- Ahnen M. L., et al., 2019, *MNRAS*, **485**, 356
- Albert A., et al., 2020, *ApJ*, **905**, 76
- Aloisio R., Berezhinsky V., Blasi P., 2014, *J. Cosmology Astropart. Phys.*, **10**, 020
- Alves Batista R., et al., 2019, *Frontiers in Astronomy and Space Sciences*, **6**, 23
- Amato E., 2014, in International Journal of Modern Physics Conference Series. p. 1460160 (arXiv:1312.5945), doi:10.1142/S2010194514601604
- Amato E., 2020, arXiv e-prints, p. arXiv:2001.04442
- Angus C. R., et al., 2019, *MNRAS*, **487**, 2215
- Arons J., 2003, *ApJ*, **589**, 871
- Asano K., Yamazaki R., Sugiyama N., 2006, *PASJ*, **58**, L7
- Berezinskii V. S., Bulanov S. V., Dogiel V. A., Ptuskin V. S., 1990, *Astrophysics of cosmic rays*
- Berezinsky V., 2014, *Astroparticle Physics*, **53**, 120
- Blasi P., 2013, *A&ARv*, **21**, 70
- Blasi P., Epstein R. I., Olinto A. V., 2000, *ApJ*, **533**, L123
- Blondin J. M., Chevalier R. A., 2017, *ApJ*, **845**, 139
- Bucciantini N., Quataert E., Arons J., Metzger B. D., Thompson T. A., 2007, *MNRAS*, **380**, 1541
- Bucciantini N., Arons J., Amato E., 2011, *MNRAS*, **410**, 381
- Burrows A., Vartanyan D., 2021, *Nature*, **589**, 29
- Bykov A. M., Marcowith A., Amato E., Kalyashova M. E., Kruijsen J. M. D., Waxman E., 2020, *Space Sci. Rev.*, **216**, 42
- Cherenkov Telescope Array Consortium et al., 2019, Science with the Cherenkov Telescope Array, doi:10.1142/10986.
- Corsi A., Lazzati D., 2021, *New Astron. Rev.*, **92**, 101614
- Coti Zelati F., Rea N., Pons J. A., Campana S., Esposito P., 2018, *MNRAS*, **474**, 961
- Cristofari P., 2021, *Universe*, **7**, 324
- Cristofari P., Gabici S., Terrier R., Humensky T. B., 2018, *MNRAS*, **479**, 3415
- Davies B., Figer D. F., Kudritzki R.-P., Trombley C., Kouveliotou C., Wachter S., 2009, *ApJ*, **707**, 844
- Delahaye T., Laval J., Lineros R., Donato F., Fornengo N., 2010, *A&A*, **524**, A51
- Devin J., Renaud M., Lemoine-Goumard M., Vasileiadis G., 2021, *A&A*, **647**, A68
- Dinnbier F., Walch S., 2020, *MNRAS*,
- Dong S., et al., 2016, *Science*, **351**, 257
- Duncan R. C., Thompson C., 1992, *ApJ*, **392**, L9
- Eichler D., 2005, arXiv e-prints, p. astro-ph/0504452
- Enoto T., et al., 2017, *ApJS*, **231**, 8
- Esposito P., Rea N., Israel G. L., 2021, in Belloni T. M., Méndez M., Zhang C., eds, *Astrophysics and Space Science Library* Vol. 461, Astrophysics and Space Science Library. pp 97–142 (arXiv:1803.05716), doi:10.1007/978-3-662-62110-3_3
- Evoli C., Blasi P., Amato E., Aloisio R., 2020, *Phys. Rev. Lett.*, **125**, 051101
- Evoli C., Amato E., Blasi P., Aloisio R., 2021, *Phys. Rev. D*, **103**, 083010
- Fang K., Murase K., 2021, *ApJ*, **919**, 93
- Fang K., Metzger B. D., Murase K., Bartos I., Kotera K., 2019, *ApJ*, **878**, 34
- Ferrand G., Safi-Harb S., 2012, *Advances in Space Research*, **49**, 1313
- Fox D. B., Kashiyama K., Mészáros P., 2013, *ApJ*, **774**, 74
- Frail D. A., Kulkarni S. R., Bloom J. S., 1999, *Nature*, **398**, 127
- Frohmaier C., et al., 2021, *MNRAS*, **500**, 5142
- Fuerst E., Reich W., Reich P., Handa T., Sofue Y., 1987, *A&AS*, **69**, 403
- Gaensler B. M., Slane P. O., 2006, *ARA&A*, **44**, 17
- Galván-Madrid R., et al., 2013, *ApJ*, **779**, 121
- Geen S., Rosdahl J., Blaizot J., Devriendt J., Slyz A., 2015, *MNRAS*, **448**, 3248
- Gnatyk R. B., 2018, *Kinematics and Physics of Celestial Bodies*, **34**, 167
- Granot J., et al., 2006, *ApJ*, **638**, 391
- Green D. A., 2019, *Journal of Astrophysics and Astronomy*, **40**, 36
- Guépin C., Kotera K., 2017, *A&A*, **603**, A76
- H. E. S. S. Collaboration et al., 2018a, *A&A*, **612**, A1
- H. E. S. S. Collaboration et al., 2018b, *A&A*, **612**, A2
- H. E. S. S. Collaboration et al., 2018c, *A&A*, **612**, A3
- H. E. S. S. Collaboration et al., 2018d, *A&A*, **612**, A5
- H. E. S. S. Collaboration et al., 2018e, *A&A*, **612**, A11
- Han J. L., et al., 2021, *Research in Astronomy and Astrophysics*, **21**, 107
- He C.-C., Ricotti M., Geen S., 2019, *MNRAS*, p. 2162
- He H.-N., Lee S.-H., Nagataki S., Kusenko A., 2020, *ApJ*, **891**, 179
- Hillas A. M., 2005, *Journal of Physics G Nuclear Physics*, **31**, R95
- Ioka K., Mészáros P., 2010, *ApJ*, **709**, 1337
- Ishizaki W., Tanaka S. J., Asano K., Terasawa T., 2017, *ApJ*, **838**, 142
- Kaplan D. L., Kulkarni S. R., Frail D. A., van Kerkwijk M. H., 2002, *ApJ*, **566**, 378
- Kargaltsev O., Cerutti B., Lyubarsky Y., Striani E., 2015, *Space Sci. Rev.*, **191**, 391
- Kashiyama K., Murase K., Bartos I., Kiuchi K., Margutti R., 2016, *ApJ*, **818**, 94
- Kaspi V. M., Beloborodov A. M., 2017, *ARA&A*, **55**, 261
- Kaspi V. M., Gavril F. P., Woods P. M., Jensen J. B., Roberts M. S. E., Chakrabarty D., 2003, *ApJ*, **588**, L93
- Kirk J. G., Duffy P., 1999, *Journal of Physics G Nuclear Physics*, **25**, R163
- Kirk J. G., Guthmann A. W., Gallant Y. A., Achterberg A., 2000, *ApJ*, **542**, 235
- Kotera K., Olinto A. V., 2011, *ARA&A*, **49**, 119
- Kotera K., Amato E., Blasi P., 2015, *J. Cosmology Astropart. Phys.*, **8**, 026
- Kouveliotou C., et al., 1998, *Nature*, **393**, 235
- Kouveliotou C., et al., 1999, *ApJ*, **510**, L115
- Krumholz M. R., McKee C. F., Bland-Hawthorn J., 2019, *ARA&A*, **57**, 227
- Lee S.-H., Patnaude D. J., Raymond J. C., Nagataki S., Slane P. O., Ellison D. C., 2015, *ApJ*, **806**, 71
- Li J., Rea N., Torres D. F., de Oña-Wilhelmi E., 2017, *ApJ*, **835**, 30
- Limongi M., Chieffi A., 2018, *ApJS*, **237**, 13
- Lin W. L., Wang X. F., Wang L. J., Dai Z. G., 2020, *ApJ*, **903**, L24
- Linden T., Auchettl K., Bramante J., Cholis I., Fang K., Hooper D., Karwal T., Li S. W., 2017, *Phys. Rev. D*, **96**, 103016
- Liu X.-W., Wu X.-F., Lu T., 2010, *New Astron.*, **15**, 292

- Lorimer D. R., Xilouris K. M., 2000, [ApJ](#), **545**, 385
- Manchester R. N., Hobbs G. B., Teoh A., Hobbs M., 2005, [AJ](#), **129**, 1993
- Marassi S., Schneider R., Limongi M., Chieffi A., Graziani L., Bianchi S., 2019, [MNRAS](#), **484**, 2587
- Martín J., Torres D. F., Rea N., 2012, [MNRAS](#), **427**, 415
- Mereghetti S., Pons J. A., Melatos A., 2015, [Space Sci. Rev.](#), **191**, 315
- Metzger B. D., Beniamini P., Giannios D., 2018, [ApJ](#), **857**, 95
- Morales E. F. E., Wyrowski F., Schuller F., Menten K. M., 2013, [A&A](#), **560**, A76
- Moriya T. J., Sorokina E. I., Chevalier R. A., 2018, [Space Sci. Rev.](#), **214**, 59
- Morlino G., Blasi P., Peretti E., Cristofari P., 2021, [MNRAS](#), **504**, 6096
- Murase K., Mészáros P., Zhang B., 2009, [Phys. Rev. D](#), **79**, 103001
- Murase K., Kashiyama K., Kiuchi K., Bartos I., 2015, [ApJ](#), **805**, 82
- Nagano M., Watson A. A., 2000, [Reviews of Modern Physics](#), **72**, 689
- Natale G., Rea N., Lazzati D., Perna R., Torres D. F., Girart J. M., 2017, [ApJ](#), **837**, 9
- Neronov A., 2017, [Physical Review Letters](#), **119**, 191102
- Olausen S. A., Kaspi V. M., 2014, [ApJS](#), **212**, 6
- Paczynski B., 1992, [Acta Astron.](#), **42**, 145
- Parfrey K., Beloborodov A. M., Hui L., 2013, [ApJ](#), **774**, 92
- Pelletier G., Bykov A., Ellison D., Lemoine M., 2017, [Space Sci. Rev.](#), **207**, 319
- Piran T., 1999, [Phys. Rep.](#), **314**, 575
- Piran T., Nakar E., Mazzali P., Pian E., 2019, [ApJ](#), **871**, L25
- Predehl P., et al., 2021, [A&A](#), **647**, A1
- Remy Q., Gallant Y. A., Renaud M., 2020, [Astroparticle Physics](#), **122**, 102462
- Reynolds S. P., 2008, [ARA&A](#), **46**, 89
- Reynolds S. P., Pavlov G. G., Kargaltsev O., Klingler N., Renaud M., Mereghetti S., 2017, [Space Sci. Rev.](#), **207**, 175
- Rice T. S., Goodman A. A., Bergin E. A., Beaumont C., Dame T. M., 2016, [ApJ](#), **822**, 52
- Sano H., et al., 2021, [ApJ](#), **919**, 123
- Slane P., Bykov A., Ellison D. C., Dubner G., Castro D., 2015, [Space Sci. Rev.](#), **188**, 187
- Sokolosky P., 2014, Report on workshop “Multimessenger Astronomy in the Era of PeV Neutrinos”, Nov 10-12, 2014, Annapolis, Maryland
- Stecker F. W., 1971, Cosmic gamma rays
- Stecker F. W., 1977, [ApJ](#), **212**, 60
- Stephenson F. R., Green D. A., 2005, [Journal for the History of Astronomy](#), **36**, 217
- Sudoh T., Linden T., Beacom J. F., 2019, [Phys. Rev. D](#), **100**, 043016
- Suzuki A., Maeda K., 2019, [ApJ](#), **880**, 150
- Tamba T., Bamba A., Odaka H., Enoto T., 2019, [PASJ](#), **71**, 90
- Tendulkar S. P., Cameron P. B., Kulkarni S. R., 2012, [ApJ](#), **761**, 76
- Testa V., et al., 2008, [A&A](#), **482**, 607
- Thompson C., Duncan R. C., 1995, [MNRAS](#), **275**, 255
- Thompson C., Duncan R. C., 1996, [ApJ](#), **473**, 322
- Torres D. F., Cillis A., Martín J., de Oña Wilhelmi E., 2014, [Journal of High Energy Astrophysics](#), **1**, 31
- Truelove J. K., McKee C. F., 1999, [ApJS](#), **120**, 299
- Turolla R., Zane S., Watts A. L., 2015, [Reports on Progress in Physics](#), **78**, 116901
- Urquhart J. S., et al., 2018, [MNRAS](#), **473**, 1059
- Vrba F. J., et al., 1996, [ApJ](#), **468**, 225
- Vrba F. J., Henden A. A., Luginbuhl C. B., Guetter H. H., Hartmann D. H., Klose S., 2000, [ApJ](#), **533**, L17
- Wachter S., Ramirez-Ruiz E., Dwarkadas V. V., Kouveliotou C., Granot J., Patel S. K., Figer D., 2008, [Nature](#), **453**, 626
- Wang Z., Li Z., Zhao Y., 2002, [ApJ](#), **569**, L43
- Wang S., Zhang C., Jiang B., Zhao H., Chen B., Chen X., Gao J., Liu J., 2020, [A&A](#), **639**, A72
- Weaver R., McCray R., Castor J., Shapiro P., Moore R., 1977, [ApJ](#), **218**, 377
- Woosley S. E., 2010, [ApJ](#), **719**, L204
- Xin S. E., Guo X. L., 2021, PoS(ICRC2021), **626**
- Yeung P. K. H., Kong A. K. H., Tam P. H. T., Lin L. C. C., Hui C. Y., Hu C.-P., Cheng K. S., 2016, [ApJ](#), **827**, 41
- Yuan Q., Lin S.-J., Fang K., Bi X.-J., 2017, [Phys. Rev. D](#), **95**, 083007
- Zabalza V., 2015, in 34th International Cosmic Ray Conference (ICRC2015). p. 922 ([arXiv:1509.03319](#))
- Zhu H., Tian W., Li A., Zhang M., 2017, [MNRAS](#), **471**, 3494
- Zhu B.-T., Zhang L., Fang J., 2018, [A&A](#), **609**, A110
- van Marle A. J., Keppens R., 2012, [A&A](#), **547**, A3
- van Paradijs J., Taam R. E., van den Heuvel E. P. J., 1995, [A&A](#), **299**, L41

This paper has been typeset from a \LaTeX file prepared by the author.